鄭澤東 敎授指導

碩士學位 請求論文

나노 다공성 표면의 전기화학적 촉매효과와 그 응용

The Electrocatalytic effect of Nanoporous Surface and its Applications

2006

誠信女子大學校 大學院

化學科

韓 枝 亨

나노 다공성 표면의 전기화학적 촉매효과와 그 응용

The Electrocatalytic effect of Nanoporous Surface and its Applications

鄭澤東 敎授指導

이 論文을 碩士學位 論文으로 提出함

2006년 5월

誠信女子大學校 大學院

化學科

韓 枝 亨

認　准　書

韓枝亨의 碩士學位 論文으로 認准함.

審査委員＿＿＿＿＿＿＿＿印

審査委員＿＿＿＿＿＿＿＿印

審査委員＿＿＿＿＿＿＿＿印

誠信女子大學校 大學院

논문 개요

본 연구에서의 나노 다공성 박막의 표면은 지름이 평균 3 nm인 수많은 동공으로 이루어져있다. 이런 특유한 구조로 인하여, 실제 면적이 평평한 표면보다 훨씬 커지고, 반응에 필요한 충돌 횟수가 증가될 것으로 예상된다. 증가된 면적에 의한 촉매 현상을 연구한 논문들은 다수 발표되어있지만, 동공 안에서 증가된 충돌수로 인한 촉매 현상을 실험적으로 증명한 논문은 발표되지 않았다. 그래서 Part I 에서는 나노 다공성 구조로 증가된 충돌횟수가 실제 반응에서 촉매작용의 한 요소로서 기여하는지를 알아보기 위하여 글루코오즈 (glucose), 과산화수소(hydrogen peroxide)의 산화반응과 pH 측정을 수행하였다. 상대적으로 반응이 느린 글루코오즈의 산화반응과 mass transport effect가 없는 pH 전위차 측정에서 나노 다공성 구조자체에 의한 촉매 현상을 확인하였다.

Part Ⅱ에서는 나노 다공성 백금의 촉매능력을 마이크로 전극에 적용하여 glutamate 효소 센서를 만들었다. 이 센서의 원리는 glutamate가 효소에 의해 분해되고, 이 반응에서 생성된 과산화수소를 백금표면에서 산화시킴으로서 그 전류를 측정하는 것이다. 지름이 25 μm인 전극에 나노 다공성 백금을 전기화학적으로 도금하고 글루타민 효소를 비전도성 폴리머인 poly-*m*-PD를 전기 중합 방식으로 전극 표면에 고정하였다. 나노 다공성 마이크로 백금 전극이 평평한 전극보다 전류가 4배 이상 큰 것을 확인하였다.

Part Ⅲ에서는 고체상 기준전극으로서 나노 다공성 백금의 가능성을 알아보고, 칩 상에서 구현하는 실험을 수행하였다. 나노 다공성 백금 산화물은 pH 반응에서 좋은 선형성과 낮은 이력현상을 보인다. 따라서 일정한 pH 환경 하에서 나노 다공성 백금은 기준전극으로서 거동할 것으로 예상된다.

poly-m-PD막을 입혀서 백금 표면의 평형반응을 방해하는 물질을 차단했고, 마이크로 칩에 적용하여 고체상 기준전극으로서의 가능성을 확인하였다.

목 차

그림 목록

Chapter I. Introduction

1. Nanotechnology

Nanotechnology is one of the most rapidly rising research fields in technology. It is the science of making things unimaginably small and gets its name from a measure of distance. A nanometer, or nano, is one-billionth of a meter. This is about the size of a cluster of atoms or small molecules, sometimes a large molecule. Nanotechnologists work with this small materials.

Many experts credit the idea to Richard Feynman, who is a well-recognized Nobel laureate physicist. In his memorial speech given in 1959, he called it "There's plenty of room at the bottom." He described the theory that scientists could make devices smaller and smaller - all the way down to the atomic level. Although he did not use the word nanotechnology, the speech got many scientists thinking about the world of the very small. But this idea remained only a theory over years since then.

At that time, no way existed to identify and/or record the structures of molecules with that size. As the nineteen eighties began, two researchers found a breakthrough. Gerd Binnig and Heinrich Rohrer, who worked at a IBM laboratory in Zurich Switzerland, invented what they called a scanning tunneling microscope (STM)[1]. This historical invention led scientists to observe molecules and even atoms in greater detail than

ever before.

Once nano-sized structures in nature started to be unveiled, the subsequent step for scientists to take was to find a way to create their own. By the middle of 1980s, scientists had focussed their research on carbon. They were especially interested in using carbon to make nano-sized structures. In 1985, Robert Curl, Harold Kroto and Richard Smalley reported a new allotrope of carbon materials. They evaporated carbon by shining laser light at a graphite surface and cooled the vapor to an extremely low temperature. From the soots, they succeeded in separating buckminsterfullerene, C_{60}, and identifying its structure that resembles a soccer ball.

The next remarkable milestone was that Japanese scientist Sumio Iijima found carbon nanotubes with six-sided atomic structures in 1993. The tubes as made were extremely strong and possessed novel properties. It is believed that nanotubes will possibly replace the carbon graphite currently being used to make airplane parts and provide new platform for various sensors, display devices, and electronic components as suggested by numerous publications[2, 3].

As for applications of nanotechnology to the computer chip, computer scientists hope that nanotechnology development will help break barriers toward computers in the next generation in terms of size and speed. In 2002, IBM announced that it had created the world's smallest transistor based on the element silicon, which was four to eight nanometers thick.

Fabrication of nano-structure with various material other than carbon

has been vigorously studied. For example, Pt, Pd, Au, Zr, and many others has been employed to make nano-structures[4-7].

2. Nanoporous metallic thin film

One of the hot issues in nanotechnology research is fabrication and application of nanoporous metal films, which has a great many of nanopores of 1 - 100 nm in diameter. Metals with nanostructures are of considerable interest for applications in catalysis, batteries, fuel cells, capacitors, and sensors[8, 9]. However, only a limited knowledge is available now in concerning how to make such films and what to be practically applied for. With respect to the fabrication, it was published that electrochemical deposition can be carried out from surfactant solution with a hexagonal lyotropic liquid crystalline phase (H_1 phase), micelle solution (L_1 phase), or below micelle concentration (*cmc*).

Attard et al. reported nanoporous platinum is obtained by electrodeposition in the *lyotropic liquid crystalline phase* (H_1 phase), consisting of the nonionic surfactant (octaethylene glycol monohexadecyl ether, $C_{16}EO_8$), hexachloroplatinic acid (H_2PtCl_6) and water[10]. Transmission electron microscopy (TEM) studies of the electrodeposited platinum (H_1-ePt) revealed a highly porous structure that had cylindrical holes 25 Å(±1.5 Å) in diameter arranged on a hexagonal lattice.

This liquid crystalline phase composed of 42 wt% of surfactant and 29 wt% of water was highly viscous so that diffusion rate towards the

electrode surface is sluggish and requires very long time for electrodeposition. Moreover, the polarization at the electrode surface is serious because of the depletion of the platinum precursor and the accumulation of byproducts such as proton and chloride ion. As a result, chemical polarization of electrochemical interface may cause poor reproducibility and uniformity of the plated films. Electrodeposition in a viscous phase brings about another problem when it comes to thin film formation on a large area. On a small surface area of the substrate electrode, for example, less than 1 mm in diameter, H_1-ePt can be uniformly electrodeposited. However, the uniformity of the plated film becomes poor as the electrode area increases.

Stucky et. al. suggested an alternative to the problematic deposition in a liquid crystalline phase by showing that the nanoporous platinum films can be prepared by the *potential-controlled self-assembly* method in dilute surfactant solutions (<*cmc*)[11]. Although the dilute surfactant solution in this method indeed allows faster electrodeposition, the corresponding nanoporous structure suffers from strong dependence upon the potential. Since the electrical field at the surface substantially affects the morphology of the plated platinum, nanoporous platinum films are not produced at a certain range of potential, at which bilayers are formed or the self-assembled structure of the surfactants are disorganized on the electrode surface.

Another electrochemical method is to deposit a metal film in the reverse micelle solution phase (L_2 phase). L_2 phase forms like that aqueous

droplets are surrounded by surfactant. At a glance it might not seem that the platinum deposition readily takes place because the aqueous regions containing platinum precursors are individually enclosed by nonpolar moieties of surfactant molecules. However, Coppola et al. reported that the proton self-diffusion was active along the neighboring aqueous domains as the water content exceeds 13 wt% in L_2 phase of binary mixture of Triton X-100 and water[12]. Thus it is conceivable that L_2 phase with relatively high water content may work as an alternative template for electroplating nanoporous metals. The high fluidity of reverse micelle solution owing to relatively high water content and the nonionic reverse micelle assembly, which is far less sensitive to any electrical field than ionic surfactants, suggest a more convenient pathway to produce nanoporous platinum electrodes. The mixture of 50 wt% Triton X-100, 45 wt% 0.3 M NaCl, and 5 wt% HCPA at 40 ℃ was identified to be a reverse micelle solution. The nanoporous platinum film as made (L_2-ePt) is predicted to have highly rough surfaces. The transmission electron microscope (TEM) images confirmed the morphology of the highly rough L_2-ePt, on which there were numerous nanopores. The diameter of nanopores is determined to be about 3 nm and the pores are densely distributed with pore-pore distance of 6 nm.

Whether nanoporous platinum is formed in liquid crystal phase or reverse micelle phase, three common characteristics are found. First, this structure provides a chance of higher collision frequency as well as enlarged active surface area. Because faradaic current is obviously

proportional to both the active surface area and collision frequency, corresponding reaction current should increase on nanoporous platinum surface. Second, it has specific pore diameter. According to IUPAC (International Union of Pure and Applied Chemistry), pore scale has classified by micropore (< 2 nm), mesopore (2-50 nm), and macropore (> 50 nm). A typical case of micropore is zeolite. Natural zeolites have a unique interconnecting lattice structure, which is arranged to form a honeycomb framework comprised of channels and pores (< 1 nm). Zeolite attracts positively charged moisture, odors and gas molecules and trap them in its crystalline structure. As molecules can enter the zeolite's pores and selectively react, zeolite generates size selective or shape selective catalytic reaction. Zeolite as a catalyst has a serious disadvantage that pore diameter is too small. It is not easy to enter bulky biomolecules (e.g. glucose, glutamate) through the zeolite's micropore. Therefore, nanoporous structure with larger pores is required for many catalytic applications. Third, the thickness of a thin film can be easily controlled by electrochemical method. If pores are too shallow, meaning those in a thin film, the catalytic effect of nanoporous structure might not be enough. On the other hand, unnecessarily deep pores make it difficult for electrochemical reaction products to escape from the nanopores. Controlling film thickness is an issue of great importance while the pore size and depth of zeolite films are hard to control. In this respect, it is a valuable aspect that the thickness of the nanoporous platinum film is governed by charge passing during the electrodeposition.

Chemical and bio-sensor is one of the promising applications using nanoporous platinum thin films. It was reported that H_1-ePt selectively enhanced the amperometric signals and thus could be utilized as a nonenzymatic glucose sensor[13]. Moreover, the nanoporosity of H_1-ePt increases the exchange current of the electrode surface and remarkably improves the performance as a pH sensing material[14].

L_2-ePt can replace H_1-ePt for glucose-, glutamate-, and pH sensors. In addition, L_2-ePt suggests some advantages over H_1-ePt. It is possible to electrochemically deposit on a large area owing to this mixture's high fluidity. And L_2-ePt is much more favorable for mass production because Triton X-100 is even cheaper than $C_{16}EO_8$, which is used for the liquid crystalline phase to make H_1-ePt.

In this study, the enhanced catalytic power of nanoporous platinum is demonstrated in terms of surface area enlargement effect and unique structural feature of nanopores. And biosensor and reference electrode based on L_2-ePt and H_1-ePt are described.

Chapter Ⅱ. Catalysis origin of the nanoporous structure

1. Introduction

Many papers addressing catalysis of the nanoporous platinum have recently reported. Birkin et al. obtained voltammograms for oxygen reduction on H_1-ePt microelectrodes[15]. They explained that highly enhanced oxygen reduction current and the positive shift of oxygen reduction onset potential are attributed to the large surface area. Evans et. al. demonstrated that H_1-ePt microelectrodes could be excellent amperometric sensors for the detection of hydrogen peroxide over a wide range of concentrations[16]. They accounted for the electrocatalytic phenomena of nanoporous platinum thin films on the basis of greatly enlarged surface area. Kucernak et al. reported application of the nanoporous platinum as a catalyst for oxygen electroreduction and methanol electrooxidation[17]. Park et al. proposed nonenzymatic glucose detection based on nanoporous platinum and ascribed selectively enhanced anodic current to the intrinsic structural feature of the nanoporous surface[13].

These papers are unequivocally saying that the electrocatalytic activity of nanoporous platinum results from the increased ratio of the apparent to real electrode surface areas, which is normally indicated by roughness factor.

This chapter addresses the novel structural effect of nanoporous

conductor surfaces by investigating amperometric responses to glucose and hydrogen peroxide, and potentiometric signals because of the pH change.

Electrochemical oxidation of glucose involves a sluggish electron transfer mechanism[18]. Hydrogen peroxide undergoes facile oxidation on platinum surface upon appropriate potential difference. Thus, glucose oxidation is kinetic-controlled while hydrogen peroxide oxidation is diffusion-controlled. The amperometric responses to the glucose oxidation are proportional to the 'real' area, namely nanoscopic surface area of the electrode. On the other hand, the oxidative current due to hydrogen peroxide is almost regardless of the nanoporous roughness[19]. Deeper and denser nanopores on an electrode surface lead to higher ratio of the nanoscopic to the apparent surface area, indicated by larger roughness factor. The nanoporous electrode exclusively enhances the faradaic currents of the sluggish reaction as depicted in Figure 1.

Figure 2 shows collision aspects at a flat and L_2-ePt electrode surface. In a flat Pt electrode surface, reactants collide with the wall in the one dimensional direction. Contrary to the flat Pt, reactants in a narrow channel of the nanoporous Pt are put into different environment in terms of collision mode. Collision frequency is obviously proportional to the probability of electron transfer at an identical experimental condition. The deep and narrow nanoporous structure significantly raises the collision frequency between the wall and reactants so that the faradaic currents of sluggish reactions should increase.

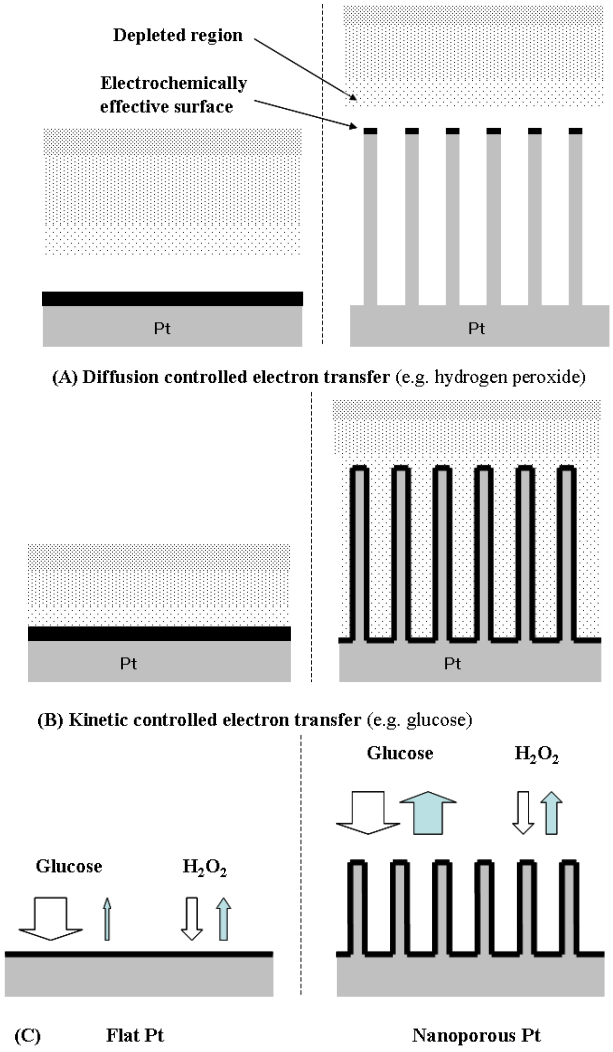

Figure 1. Schematic representation of the effect of the porous structure on electrochemical reactions.

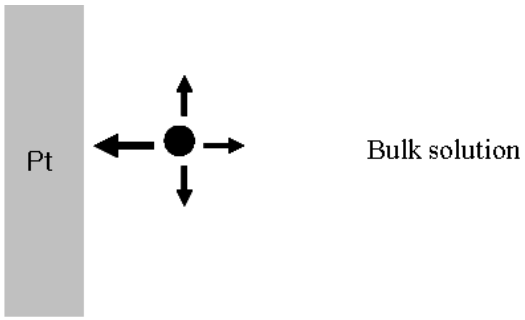

(A) Collision trend at a flat Pt electrode surface (one – dimension)

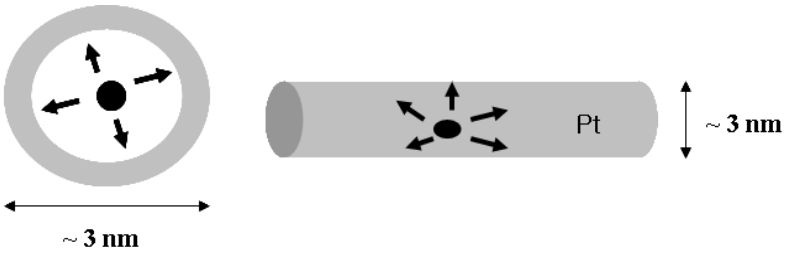

(B) Collision trend at inner wall of a nanoporous Pt electrode (three – dimensions)

Figure 2. Schematic representation of collision trends at a flat Pt and L_2-ePt.

This architectural effect of the nanoporous structure can be applied to potentiometric sensing in a similar manner. Potentiometric pH response attains by measuring open circuit potential (E_{oc}), which is defined as the potential when net current is zero. Ideally, a potentiometric sensor should have at least one nonpolarizable interface, on which any particular current does not produce further overpotential. That is why E_{oc} measurement is more reliable at less polarizable sensing interface. The equilibrium exchange current density, i_0, is a quantitative criterion of polarizability[20]. It is evident that the electrode/solution interface becomes proportionally less polarizable as i_0 climbs. The E_{oc} of metal/metal oxide is determined by the equilibrium between the metal/metal oxide and proton. It was previously reported that the E_{oc} at the interfaces of metal oxides depends on the redox equilibrium as the follow[21].

$$MO_X + 2\delta H^+ + 2\delta e^- \leftrightarrows MO_{X-\delta} + \delta H_2O$$

Since metal/metal oxide equilibria are basically established in confined surface reactions, i_0 should be proportional to the surface area. If the area of the flat electrode is not large enough to produce a sufficiently high i_0, E_{oc} will be unstable. In addition to the enlargement of the electrode area, the geometric feature of nanopores may contribute to raise i_0. Higher collision frequency of the protons by active sites on the nanopores′ wall provides fast response time and more stable open circuit potential. Consequently, nanoporous platinum structure is expected to respond more quickly, sensitively, and reproducibly to pH variation by

its extremely large real area and high collision frequency.

The nanoporous platinum oxide (H_1-ePtO) as a hydrogen ion-selective sensing material was reported[14]. According to the report, bare nanoporous platinum oxides exhibit near-Nernstian behavior (e.g., -55 mV/pH in PBS), ignorable hysteresis, a short response time, and high precision, which are remarkably better than those of flat platinum oxides. However, geometric effect of the nanopores could not be verified because pH responses were recorded using H_1-ePt and flat Pt with identical apparent area and different real area. This study was aimed to show and investigate the surface geometric effect of the nanoporous thin films.

L_2-ePt was used throughout the experiments. L_2-ePt has no property that is different from H_1-ePt except fabrication procedure. Rather, L_2-ePt is convenient to handle. For example, electrodeposition in the reverse micelle solution is far easier than that of H_1-ePt and produces more uniform surface when applied on large area.

2. Experimental

2.1. Reagents

Hydrogen hexachloroplatinate hydrate (Aldrich, 99.995 %), triton X-100 (t-Octylphenoxypolyethoxyethanol, Sigma), sodium chloride (Junsei chemicals Co., LTD., 99.5 %), sulfuric acid (YAKURI PURE CHEMICALS CO., LTD., 85 %), NaH_2PO_4(DAE JUNG Co., LTD., 98.0 %), $Na_2HPO_4 \cdot 12H_2O$(DAE JUNG Co., LTD., 98.0 %), potassium chloride, H_3PO_4(YAKURI PURE CHEMICALS CO., LTD., 85 %), hydrogen peroxide(Junsei chemicals Co., LTD., 30 %), D-(+)-glucose (sigma), Na_3PO_4(Aldrich, 96 %) were used without further purification.

2.2. Instruments

Electrochemical experiments were performed using an electrochemical analyzer (model CH 660, CH Instruments Inc., Austin, TX 78733). Ag/AgCl (saturated KCl) or Hg/Hg_2SO_4 (saturated K_2SO_4) and a platinum wire (dia. 0.5 mm) were used as reference and counter electrodes, respectively. In electrochemical tests for H_2O_2 and glucose, platinum rod electrodes (dia. 1 mm) were used as a substrate electrode for the nanoporous platinum film and flat electrode. In pH test, a platinum microelectrode (dia. 25 μm) and a platinum rod electrode (dia. 0.25 mm) were used as a substrate electrode for the nanoporous

platinum film and flat electrode, respectively. E_{oc} measurements were carried out using a homemade multipotentiometer. A combination pH electrode (ROSS 8102, Orion) was used to check solution pHs during E_{oc} measurements.

2.3. Preparation of reverse micelle solution

Triton X(Tx-100) 50 wt%, 0.3 M NaCl 45 wt%, and hydrogen hexachloroplatinate hydrate 5 wt% were mixed and the temperature was raised to 60 ℃, at which point the mixture becomes transparent and homogeneous. And the temperature was lowered to room temperature (23-26 ℃)

2.4. Electrodeposition of nanoporous platinum

Platinum deposition was carried out on a polished platinum rod electrode at constant potential (-0.2 V vs Ag/AgCl) in reverse micelle solution sustaining temperatures of nearly 40 ℃. The resulting nanoporous platinum electrode was placed in distilled water for 1 h to extract the Tx-100, and the extraction procedure was repeated 3-4 times. The electrode was then electrochemically cleaned using a cycling potential between 0.68 and -0.72 V versus Hg/Hg_2SO_4 in 1 M sulfuric acid until reproducible cyclic voltammograms were obtained.

2.5. Electrochemical experiments

The surface areas of the Pt electrodes were determined by measuring the areas under the hydrogen adsorption/desorption peaks of the cyclic voltammograms (scan rate, 200 mV/s) in 1 M sulfuric acid solution. A conversion factor of 210 μC/cm^2 was used to determine the electrode area[22].

The nanoporous platinum electrode was evaluated as a glucose sensor in aerated 0.1 M phosphate buffered saline (PBS) solution containing 0.15 M NaCl and in a cell containing 5 mL of PBS (pH 7.4). Amperometric curves were obtained in a quiescent solution a few seconds after stopping the stirring that was required to mix the materials added (i.e., glucose, H_2O_2). Current changes 100 s after adding glucose to concentrations of 1, 3, 6, 10, 15, and 20 mM were treated as specific responses to the glucose in the solution. Each experiment was conducted after drying platinum electrodes, which were electrochemically cleaned in 1 M sulfuric acid, for a day in the air.

A platinum oxide layer should be formed on the electrode surface for potentiometric pH sensing. To do so, 0.6 V versus Ag/AgCl was applied to L_2-ePt and flat Pt electrodes in PBS solution(pH 7.4) for 600 s. And the electrodes were stabilized in PBS solution for a half day. And pH measurements were conducted in stirred solutions using L_2-ePtO and flat PtO as working electrode and an Ag/AgCl(saturated KCl) as reference electrode.

3. Results and Discussions

3.1. Characterization of nanoporous platinum

The platinum film electroplated from a reverse micelle solution (L_2-ePt) has tremendously extended surface area just like that from the H_1 phase (H_1-ePt). The cyclic voltammograms of the flat Pt and L_2-ePt electrodes show the typical redox behavior of platinum itself and the adsorption and desorption of hydrogen in H_2SO_4 solution (Figure 3).

From the peak area of hydrogen adsorption, roughness factors of the electrodes were calculated with the fact that a monolayer of hydrogen corresponds to about 210 $\mu C/cm^2$ for real surface area. Figure 4 shows that the roughness factor is proportional to the charge that passed during L_2-ePt electrodeposition. This result indicates that pores are open, and the inner walls of pores are exposed, for the most parts, to the solution. Thus the pores act as electrochemically active surface.

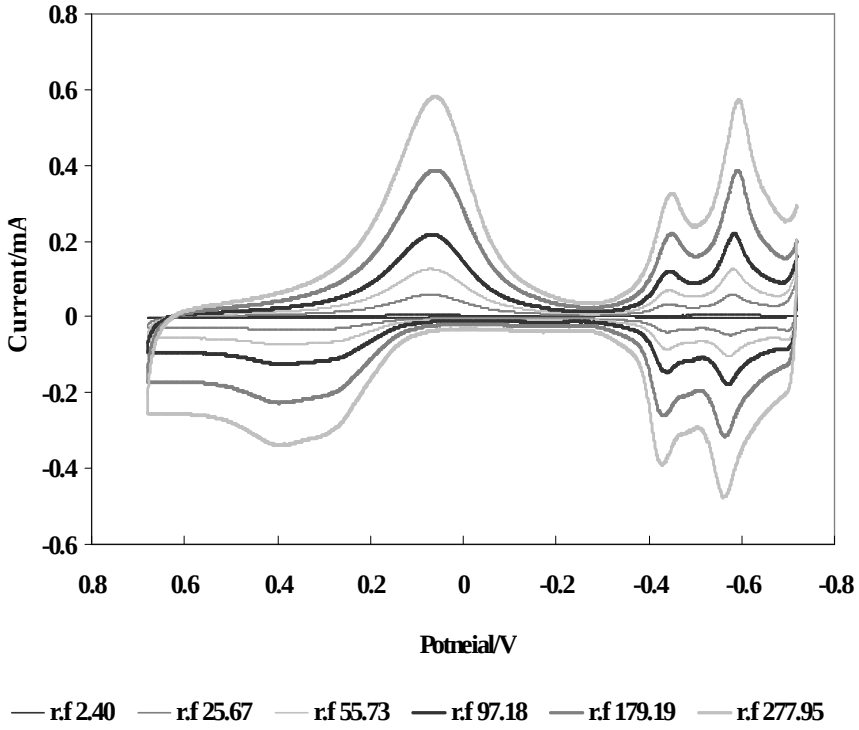

Figure 3. Cyclic voltammograms of flat Pt (r.f 2.40) and L_2-ePt electrodes having various roughness factors in 1 M H_2SO_4 at the scan rate of 200 mV/s.

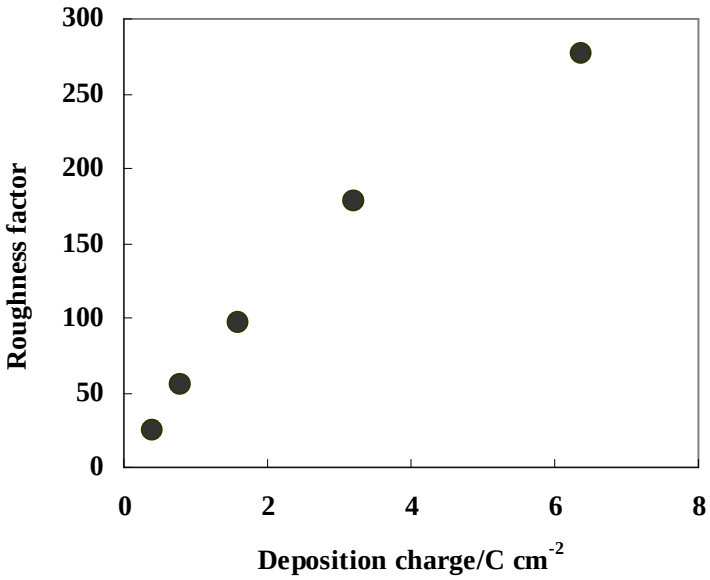

Figure 4. Plot of roughness factor vs. charge passed for L_2-ePt deposition.

3.2. Amperometric response to glucose and hydrogen peroxide

Amperometric measurements were performed at 0.5 V versus Ag/AgCl, which was positive enough to oxidize glucose and hydrogen peroxide. L_2-ePt electrodes with various roughness factors were formed by controlling the charge passed during the deposition process. These electrodes were then used to measure the signals for glucose and hydrogen peroxide.

Figure 5 shows that linear dependence of the responses of L_2-ePt to glucose concentration on the roughness factors. Because y axis is the current divided by apparent surface area, this plot implies that enhanced surface area has strong effect on glucose oxidation.

Figure 6 explains the effect of geometric factor on L_2-ePt. Expended surface area is excluded because current was divided by real surface area. Roughness factor therefore means the density of pores. Large roughness factor implies that collision frequency in the inner wall of the nanoporous structure is greater than that flat Pt. As roughness factor increases by, signals also increase. So, it indicates that geometric factor clearly exists in the catalysis of the nanoporous Pt on sluggish redox reactants.

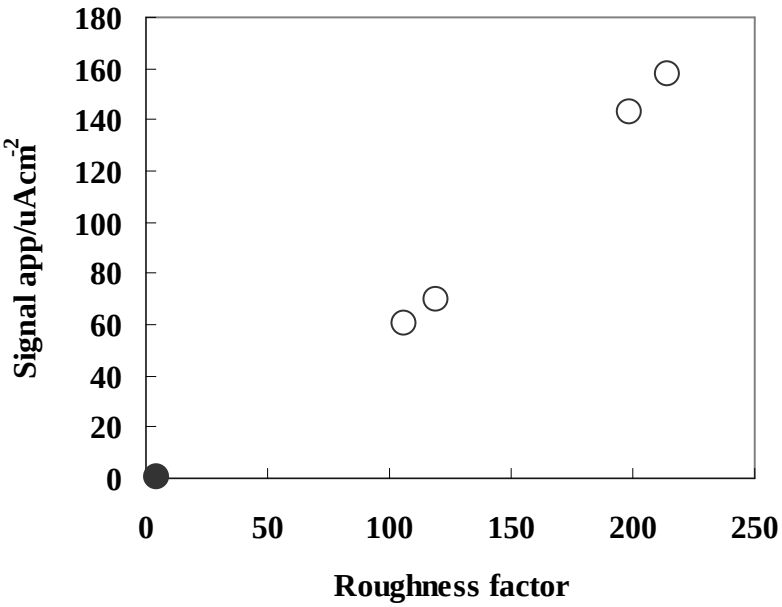

Figure 5. Effect of the roughness factor of L_2-ePt and flat Pt on the signals for 6 mM glucose. Y axis is the current divided by apparent surface area. The signals were determined in quiescent solutions 100 s after adding glucose.

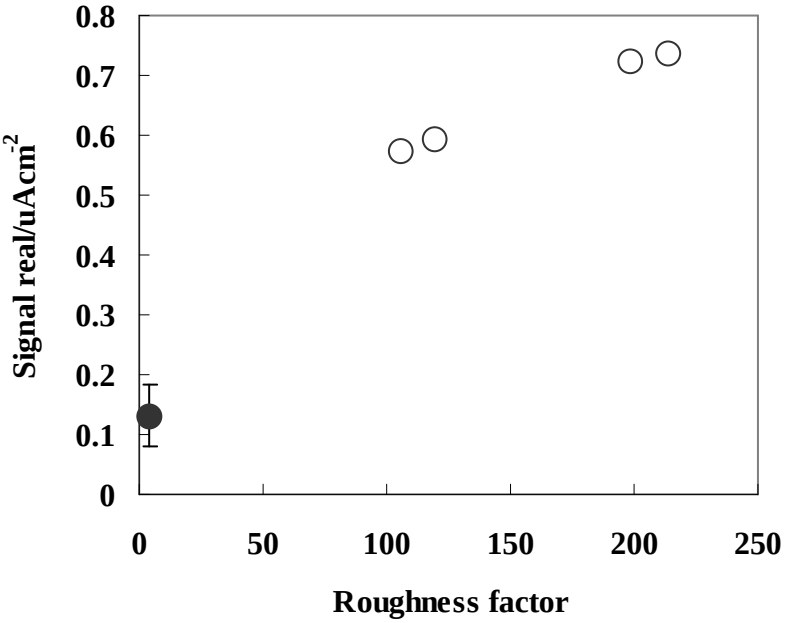

Figure 6. Effect of the geometric factor of L_2-ePt and flat Pt on the signals for 6 mM glucose. Y axis is the current divided by real surface area. The signals were determined in quiescent solutions 100 s after adding glucose.

Oxidation of hydrogen peroxide for roughness factor is a contrast to that of glucose. For all roughness factors increase, the signal of flat Pt is similar to that of L_2-ePt (Figure 7). Figure 8 shows that currents divided by real area are in inverse proportion to roughness factors. These results indicate that diffusion-controlled hydrogen peroxide oxidation almost occurs at outside of electrode surface before entering reactants in the inside of the pore. That is to say, geometric catalytic effect of nanoporous structure doesn't appear on rapidly oxidizable or reducible reactants.

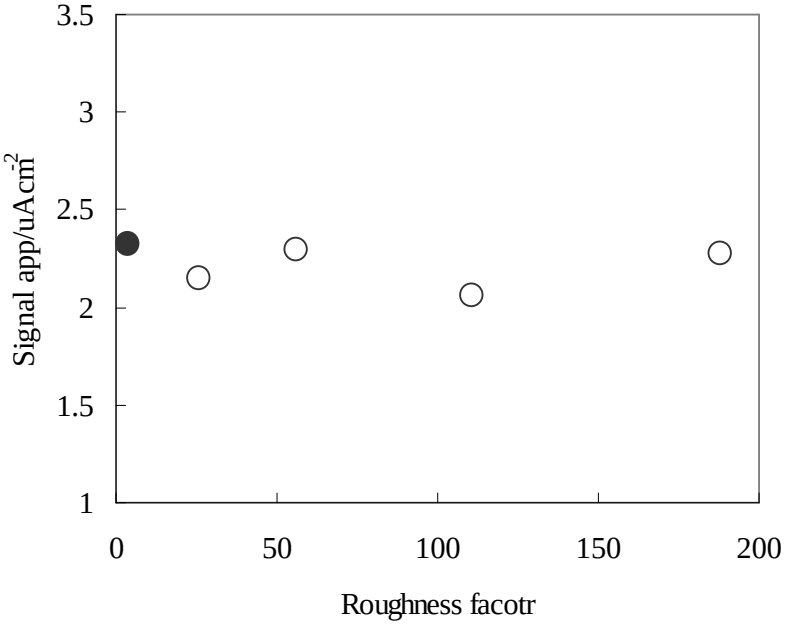

Figure 7. Effect of the roughness factor of L_2-ePt and flat Pt on the signals for 30 μM hydrogen peroxide. Y axis is the current divided by apparent surface area. The signals were determined in quiescent solutions 100 s after adding hydrogen peroxide.

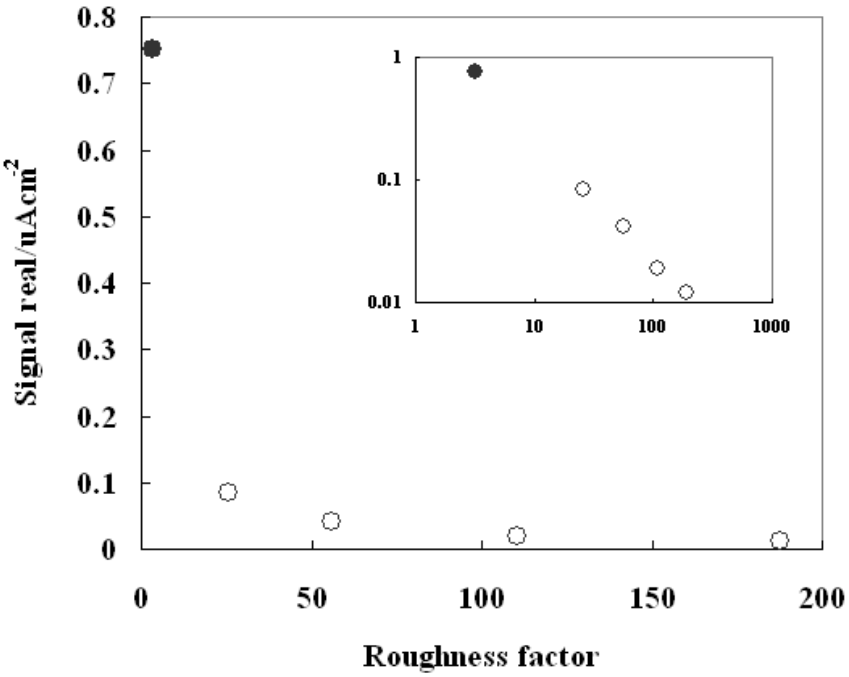

Figure 8. Effect of the geometric factor of L_2-ePt and flat Pt on the signals for 30 μM hydrogen peroxide. Y axis is the current divided by real surface area. The signals were determined in quiescent solutions 100 s after adding hydrogen peroxide. Inset: Logarithmic scale for this plot.

3.3. Potentiometric response to pH

Figure 9 shows potentiometric response of L_2-ePt (dia. 25 μm) and flat Pt (dia. 0.25 mm) to a pH shift from 7.4 to 2.0. Real area of L_2-ePt (5.976×10^{-4} cm^2) is smaller than flat Pt (1.371×10^{-3} cm^2). But pH response time ($T_{95\%}$ of ~ 60 s) of L_2-ePt is faster than flat Pt ($T_{95\%}$ of ~ 200 s). Although real area of nanoporous surface is small, numerous nanopores offer high collision frequency of proton in its active sites and fast Pt/PtO equilibrium. Accordingly, architectural of nanoporous surface accelerates pH response time and provides more stable open-circuit potential.

Figure 10 shows the effect of nanoporous structure on pH linearity and slope. L_2-ePtO shows good linearity over a wide pH range from 2 to 12, whereas flat Pt deviate seriously from linearity. And the pH response of L_2-ePtO exhibits near Nernstian behavior with a slope of -51 mV/pH. But flat PtO has a poor slope of -42 mV/pH. Consequently, architecture with many nanopores is another reason why the nanoporous platinum thin film works well as a pH sensor, though real area of nanoporous platinum is smaller than flat Pt.

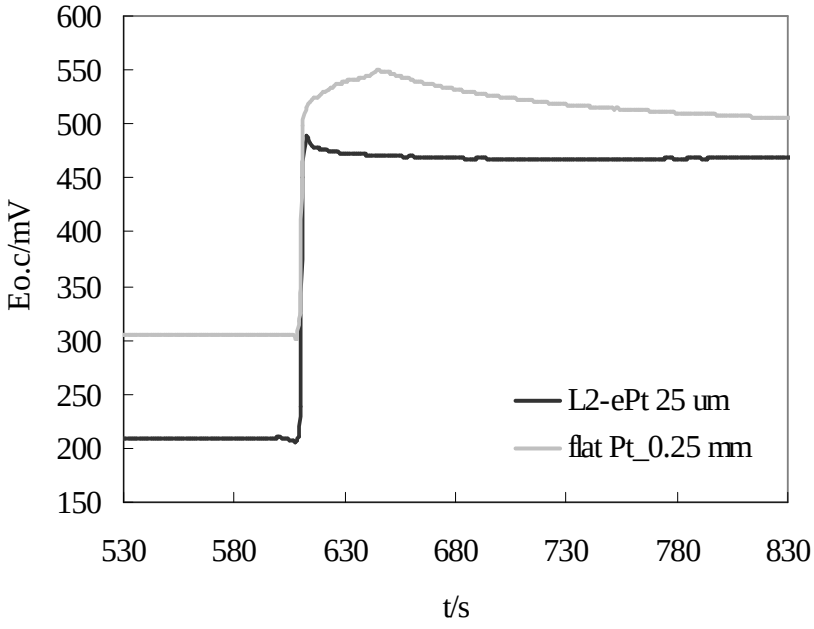

Figure 9. Potentiometric response of L_2-ePtO and flat PtO to a pH shift from 7.4 to 2.0. E_{oc} was recorded in aerated and stirred PBS solution. Real area : L_2-ePtO (5.976×10^{-4} cm^2), flat PtO (1.371×10^{-3} cm^2)

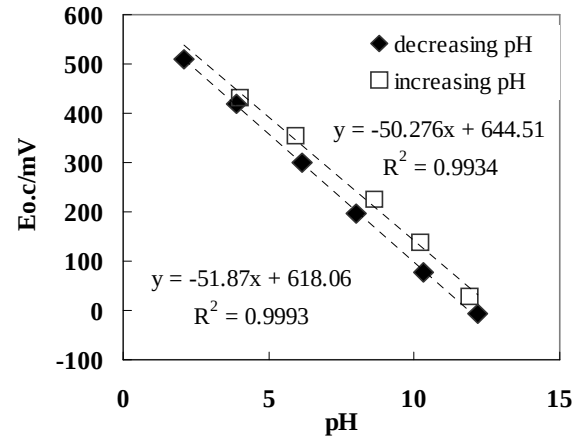

(A)

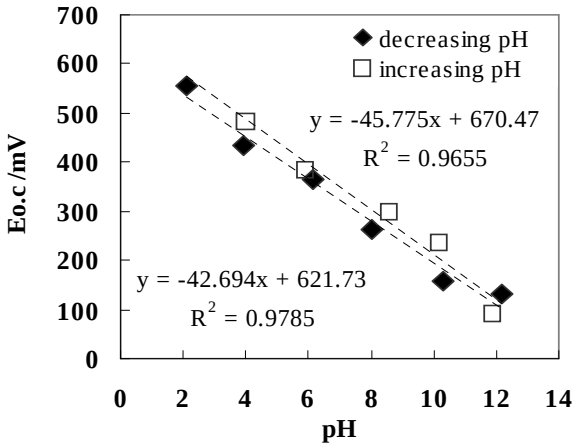

(B)

Figure 10. E_{oc} versus pH curves of L_2-PtO (A) and flat PtO (B). pH was decreased by adding 2 M H_3PO_4 to 0.1 M Na_3PO_4 (diamond) and then increased by adding 2 M NaOH again (square).

Real area : L_2-ePtO (5.976×10^{-4} cm^2), flat PtO (1.371×10^{-3} cm^2)

4. Conclusions

We investigated electrocatalysis of the nanoporous structure in terms of high collision frequency as well as enhanced surface area by examining amperometric and potentiometric behavior.

Faradaic current on a flat planar electrode is obviously proportional to the surface area. However, diffusion-limited system involving fast electron transfer produces amperometric responses that is not a function of nanoporosity, normally indicated by roughness factor. On the other hand, when it comes to sluggish reaction such as electrochemical oxidation of glucose, the faradaic current sensitively depends on the nanoscopic surface area. The amperometric responses to reactants in kinetic-controlled system can be selectively amplified over interfering species undergoing facile electron transfer by introducing nanoporous structure. As for glucose oxidation, a nanoporous electrode can produce even larger current than a flat one with the identical apparent area does. And the amplification magnitude reaches several hundred times depending on the roughness factor. These results are unambiguously attributed to the enlargement of the real surface area due to nanoporous structure. However, the detailed experiments in this study shows that collision frequency enhancement driven by the structural feature is another origin. Even if a nanoporous and a flat platinum electrodes are set to have an identical real surface area, the current from the flat Pt is not as high as that from the nanoporous Pt.

Potentiometric responses reveal another aspect of nanoporous surface effect, in which no mass transfer but surface equilibrium is involved. In practice, L_2-ePt with smaller real surface than flat Pt showed faster response time, better linearity, and near-nernstian slope, all of which are owing to unique nanoporous structure.

Chapter Ⅲ. Electrochemical Oxidation of Hydrogen Peroxide at Nanoporous Platinum Electrodes and the Application to Glutamate Microsensor

1. Introduction

Nanoporous platinum has received much attention with regard to its potential applications. Corresponding research efforts have produced a number of impressive applications[13-14, 15, 17, 23-28], one of which is applicability of nanoporous platinum for the enhancement of hydrogen peroxide (H_2O_2) redox current[16]. Although accurate and reliable detection of H_2O_2 is of interest in many fields, it has not been easy to detect H_2O_2 accurately with amperometric techniques because its electrode reactions are complicated and voltammograms tend to be irreproducible at the majority of electrode surfaces[29, 30].

A mechanism for the oxidation of H_2O_2 at platinum electrodes has recently been discussed in detail and provides an adequate explanation for the lack of linearity observed in the electrode response. Hall et al., in a series of their papers[31-35], reported that the current response due to H_2O_2 oxidation is under mixed kinetic and diffusion control.

Glutamate is an important neurotransmitter in the mammalian central nervous system, and neuronal pathways in the brain that use glutamate as a transmitter are heavily implicated in several neurological disorders such as schizophrenia, Parkinson's disease, epilepsy, and stroke[36, 37].

These pathways are also involved in drug abuse and addiction. Accurate information about the dynamic levels of glutamate in the extracellular spaces of living brain tissue would make a significant contribution to our fundamental understanding of the role of glutamate in these disorders, and helps advance therapeutic strategies. Thus the sensitive and selective glutamate microsensor is in great demand to collect temporal variation of glutamate on a real time basis. The most typical method of glutamate biosensor is to make enzyme electrode by immobilizing glutamate oxidase on to a substrate electrode such as platinum. The information of glutamate concentration is extracted from the amperometric oxidation current of H_2O_2 as a product of the enzyme reaction. That is why the enhancement of H_2O_2 oxidation current is the key issue to obtain better glutamate microbiosensor.

We describe here electrochemical behavior of H_2O_2 at nanoporous platinum (L_2-ePt) microelectrodes with a variety of area, and the apparent electrocatalytic effect in terms of H_2O_2 redox processes. And the glutamate micro-biosensor based on nanoporous Pt was developed and discussed in comparison with that based on flat platinum.

2. Experimental

2.1. Reagents

All the chemicals including hydrogen hexachloroplatinate hydrate (Aldrich), triton X-100(Tx-100) (Aldrich), sodium chloride (Aldrich), 1,3-phenylenediamine(*m*-PD) (Aldrich), L-glutamate oxidase (Yamasa Co.) were used without further purification. 1 mM 1,3-phenylenediamine and 0.025 % glutaldehyde aqueous solutions were utilized for enzyme immobilization. All electrochemical tests for H_2O_2 and glutamate were carried out in a temperature-controlled cell, which has 10 mL of 0.1 M phosphate buffered saline (PBS) containing 0.15 M NaCl at pH 7.4 and 37 ± 0.2 °C.

2.2. Instruments

All electrochemical measurements were performed in a three-electrode system. Potentiostat for electrochemical experiments was an electrochemical analyzer (Model CH750, CH Instruments Inc. Austin, TX). Reference electrode and counter electrode were an Ag/AgCl and a platinum wire, respectively. As working electrodes, nanoporous platinum microelectrodes were prepared using teflon-coated Pt-Ir alloy wires with three different diameter of 25, 76 and 178 μm. A commercialized flat platinum disk microelectrode with 25 μm in diameter was purchased from

CH Instruments Inc.

2.3. Preparation of reverse micelle solution

Tx-100 50 wt%, 0.3 M NaCl 45 wt%, and hydrogen hexachloroplatinate hydrate 5 wt% were mixed, and the temperature was raised to 60 ℃, at which point the mixture becomes transparent and homogeneous. And the temperature was lowered to room temperature (23-26 ℃)

2.4. Electrodeposition of nanoporous platinum

Platinum was deposited on a polished Pt-Ir alloy electrodes at constant potential (-0.2 V vs. Ag/AgCl) in reverse micelle solution. The resulting nanoporous platinum electrode was placed in distilled water for 1 h to extract the T_X-100, and the extraction procedure was repeated 3-4 times. The electrodes were then electrochemically cleaned using a cycling potential between 1.0 V and -0.45 V versus Ag/AgCl in 1 M sulfuric acid until reproducible cyclic voltammograms were obtained.

2.5. Glutamate oxidase immobilization

In order to immobilize glutamate oxidase (GLOx) on flat or nanoporous Pt, electrodes were immersed in a solution containing 2.5 mg GLOx, 0.0025 % glutaraldehyde, and 1 mM 1,3-phenylenediamine.

1,3-phenylenediamine was electropolymerized on the electrode and GLOx was entrapped inside polymer network during voltage cycling from 0.2 V to 0.7 V at a scan rate of 10 mV/s, 2 segment.

3. Results and Discussions

3.1. Characterization of nanoporous platinum

Nanoporous Pt was electrodeposited in a T_X-100 based reverse micelle phase. In case of electrodeposition on electrode with microscale surface, it is easy to fabricate in fluidic reverse micelle (L_2) phase. The Pt films as obtained were confirmed by checking cyclic voltammograms of the nanoporous Pt, which have tremendously large hydrogen adsorption/desorption peaks (r.f 300) (Figure 11).

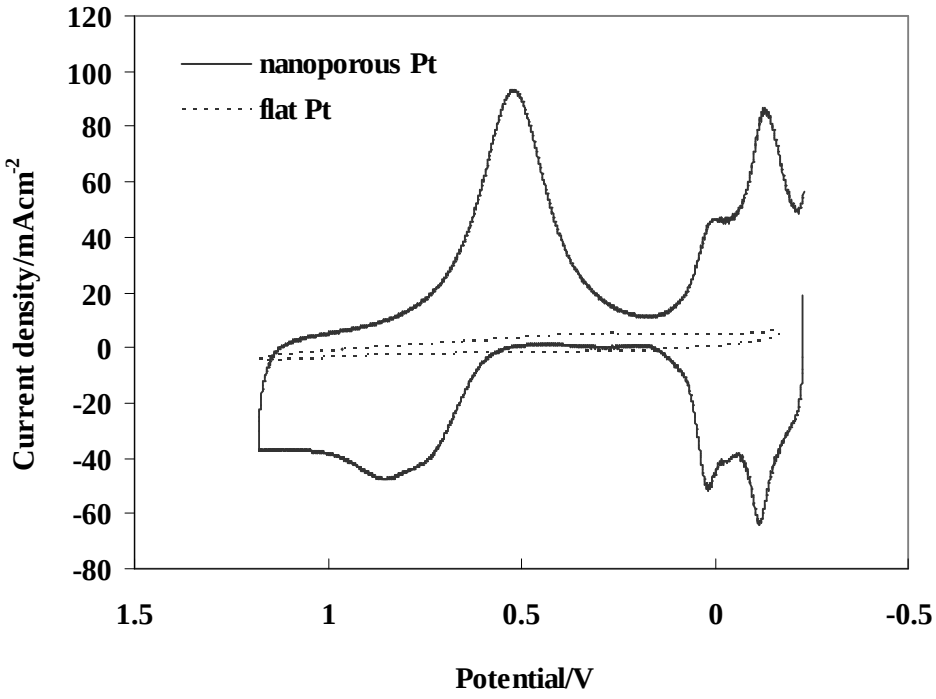

Figure 11. Cyclic voltammograms of a flat platinum and a nanoporous platinum electrode in 1 M H_2SO_4

3.2. Oxidation of H_2O_2 at flat and nanoporous Pt in PBS

Fig. 12 shows the H_2O_2 - involved electrochemical behavior from flat and nanoporous Pt microelectrodes. The voltammogram of the flat electrode is different from that of typical diffusion-controlled reaction at microelectrode. The flat microelectrode gives negligible oxidation current in this potential window and ill-defined reduction current. The electrochemical behavior of H_2O_2 at flat Pt microelectrode is kinetic-controlled.

This is not surprising because the electron transfer of H_2O_2 at a flat Pt microelectrode is not fast enough to meet the inbound spherical flux from the bulk solution. In contrast, the linear sweep voltammogram of nanoporous Pt electrode produces the well-defined plateau for both oxidation and reduction of aqueous H_2O_2 at pH 7.4. The onset potential of H_2O_2 oxidation at nanoporous Pt shifted in less positive direction so that the considerable current for H_2O_2 oxidation is observed around 0.35 V where oxidation current at flat Pt is almost zero. Moreover the limiting currents of the nanoporous Pt are much higher than that of flat Pt. These results unequivocally indicate that the redox processes of H_2O_2 at nanoporous Pt are controlled by diffusion while those at the flat Pt is kinetic controlled.

It is believed that such enhancement of faradaic currents and onset potential shift of H_2O_2 oxidation resulted from the catalytic ability of nanoporous Pt. There are a lot of nanopores on the nanoporous Pt

surface, which provide more favorable condition for H_2O_2 oxidation. First of all, nanoporous surface has tremendously enlarged area that can participate in faradaic reaction. The roughness factor, which was determined by voltammogram in 1 M H_2SO_4, shows several hundreds times larger area of the nanoporous electrode than that of the flat one with the identical apparent area. In addition, it is probable that the geometric effect of nanopores is also responsible for the enhancement of faradaic current. The narrow pore structure offers much more chances to collide with the inner wall. The concerted effect of the enlarged area and the geometric feature makes H_2O_2 redox process, especially oxidation, fast enough for the voltammetric behavior to be diffusion-controlled in spite of the high flux due to spherical diffusion at the microelectrode.

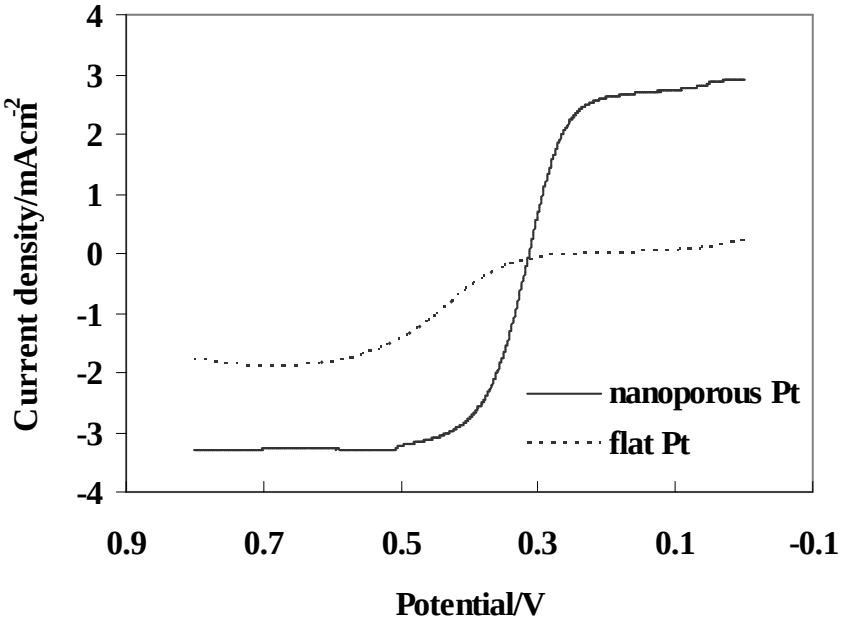

Figure 12. Linear sweep voltammograms of 1 mM H_2O_2 in PBS at a flat and a nanoporous Pt electrodes of 25 μmin diameter.

Fig. 13 is the linear sweep voltammograms of H_2O_2 oxidation at nanoporous Pt with the diameters of 25 μm, 76 μm, and 178 μm, respectively. The roughness factors were controlled to be 300 (299±16) in order to observe the effect of electrode area to the current density. As the electrode area increases, the oxidation and reduction currents grow with the same plateau shape. The reaction rate of H_2O_2 is fast enough at the nanoporous Pt surface. Namely, the reaction is diffusion-controlled. However, in terms of the current density, the trend is inversed. The calculated current densities are 3.28 x 10^{-3} A/cm^2 (25 μm), 1.80 x 10^{-3} A/cm^2 (76 μm), and 7.94 x 10^{-4} A/cm^2 (178 μm), respectively. Larger electrode area produces lower current density. It is ascribed to the contribution of spherical diffusion at the micro-disk electrode. As the electrode area is enlarged, or the microelectrode becomes semi-microelectrode, the fraction of lateral diffusion to planar mass transport becomes lowered. As a result, the inbound flux of H_2O_2 per unit electrode area decreases as it becomes more like 1-D planar diffusion system.

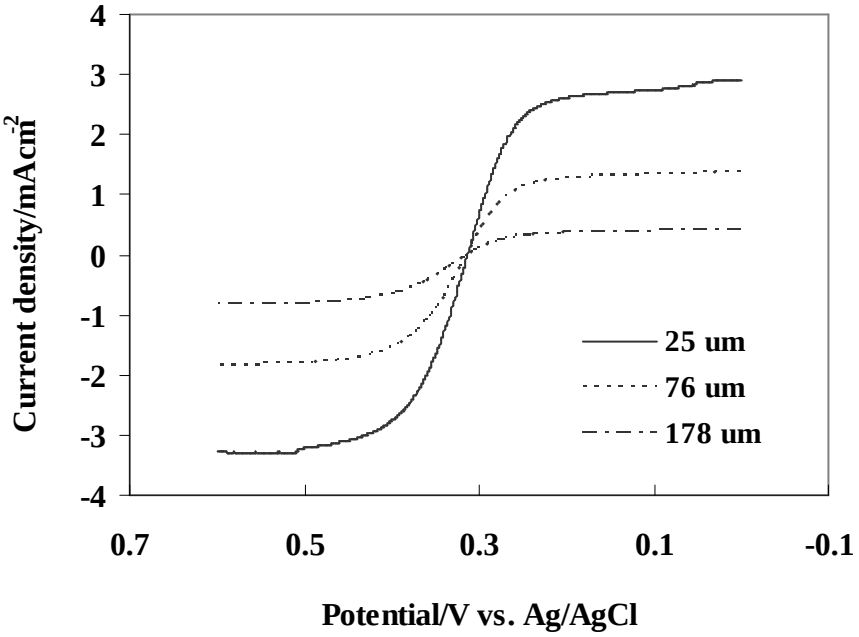

Figure 13. Linear sweep voltammograms of oxidation of 1 mM H_2O_2 in a deaerated PBS solution at pH 7.4 from nanoporous Pt electrodes with various diameters, 25 μm (roughness factor: 299), 76 μm (288), and 178 μm (320), respectively. Scan rate is 1 mV/s.

3.3. Effect of the poly *m*-PD membrane on H_2O_2 oxidation

Figure 14 is the linear sweep voltammograms of H_2O_2 oxidation at poly *m*-PD deposited flat and nanoporous Pt with the diameters of 25 μm. Compared with bare nanoporous Pt, the presence of poly *m*-PD on the nanoporous Pt makes skewed and reduced the well-defined plateau of the voltammogram. This is attributed to slow diffusion rate of H_2O_2 through the dense poly *m*-PD membrane. Although oxidation and reduction current of H_2O_2 at poly *m*-PD deposited nanoporous Pt is smaller than that of bare nanoporous Pt, it is still far larger than that of poly *m*-PD deposited flat Pt. Accordingly, one can see the enhancement in faradaic current due to nanoporous structure even in the presence of poly *m*-PD membrane for enzyme immobilization.

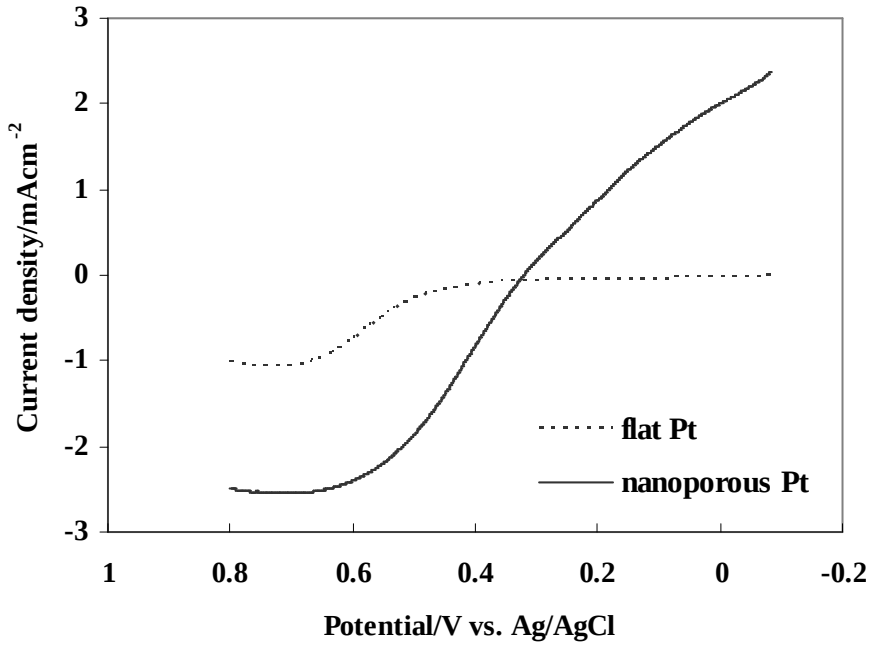

Figure 14. Linear sweep voltammograms of 1 mM H_2O_2 in PBS at a poly *m*-PD membrane coated flat and nanoporous Pt electrodes of 25 μm in diameter. Scan rate is 1 mV/s.

3.4. Amperometric detection of H_2O_2 and glutamate

In order to show the applicability to H_2O_2 sensor, amperometric measurement of H_2O_2 was carried out at both flat and nanoporous Pt electrodes. Applied potential was 0.4 V vs. Ag/AgCl, at which limiting current could be acquired. Figure 15 shows that the slope of calibration curve at the flat Pt was 2.4 pA per 10 μM and that at the nanoporous Pt was 9.7 pA per 10 μM. Thus, nanoporous Pt was more sensitive for H_2O_2 than flat Pt by four times in this experiment.

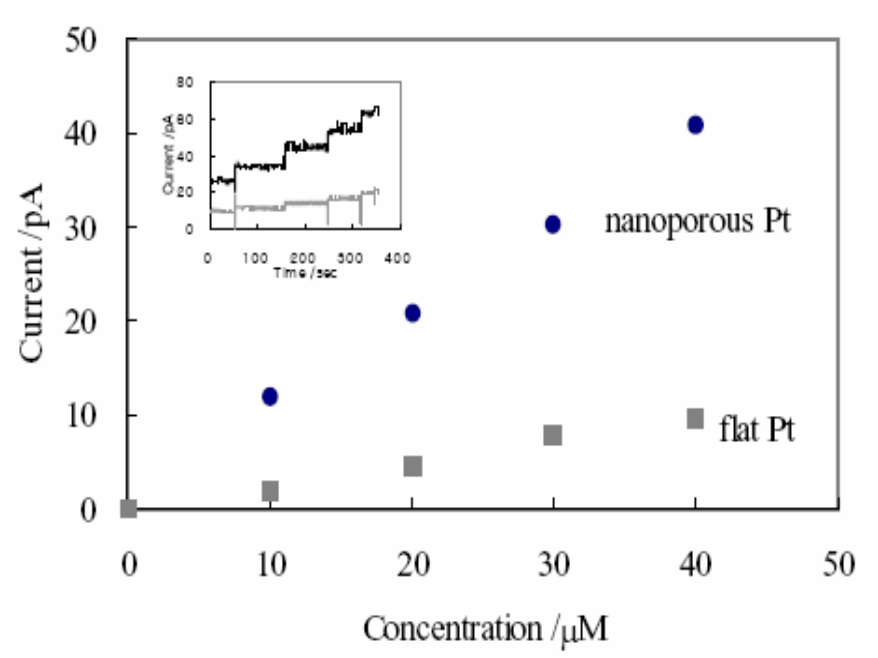

Figure 15. Calibration curves for amperometric detection of H_2O_2 at flat and nanoporous Pt. The diameter of the electrodes was 25 μm. The inset shows the raw signals from amperometric measurements.

H_2O_2 is a product of various enzyme reactions in metabolism. In this study, a microsize enzymatic biosensors were manufactured by entrapping glutamate oxidase on flat and nanoporous Pt electrodes during electropolymerization of 1,3-phenylenediamine. The oxidation of glutamate by glutamate oxidase (GLOx) produces stoichiometric amount of H_2O_2 and α-ketoglutarate so that the concentration of glutamate can be determined from the electrochemical oxidation current of H_2O_2. The reactions taking place at the electrode are as follows;

$$L-\text{glutamate} + O_2 + H_2O \xrightarrow{GLOx} \alpha-\text{ketoglutarate} + H_2O_2 + NH_3$$
$$H_2O_2 \rightarrow 2H^+ + O_2 + 2e^-$$

The schematic diagrams of enzymatic glutamate sensors prepared on flat and nanoporous Pt are shown in Figure 16. H_2O_2 as a product of the enzyme reaction is oxidized at the Pt surface. It is conceivable that nanoporous Pt could catalyze the electron transfer reaction of H_2O_2 oxidation. If so, glutamate sensor based on nanoporous Pt would produce larger responses to glutamate than that based on flat Pt.

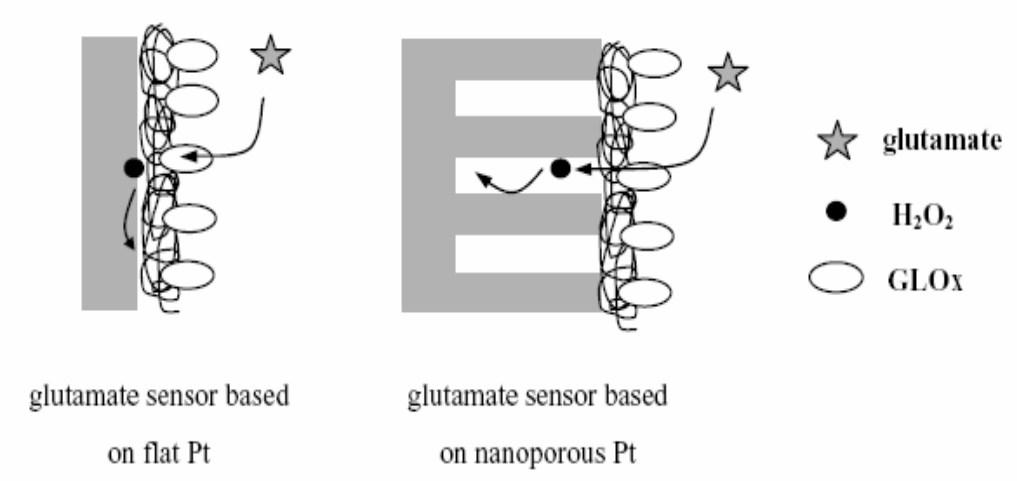

Figure 16. Schematic diagram of enzymatic glutamate sensor based on flat and nanoporous Pt electrodes.

Figure 17 shows how the enzymatic biosensors manufactured on flat and nanoporous Pt respond to L-glutamate. The slopes of the calibration curves for flat and nanaporous Pt are 2.0 pA per 10 μM and 7.6 pA per 10 μM, respectively. The sensitivity of nanoporous Pt for glutamate is four times higher than that of flat Pt, which is similar to the result of H_2O_2 detection.

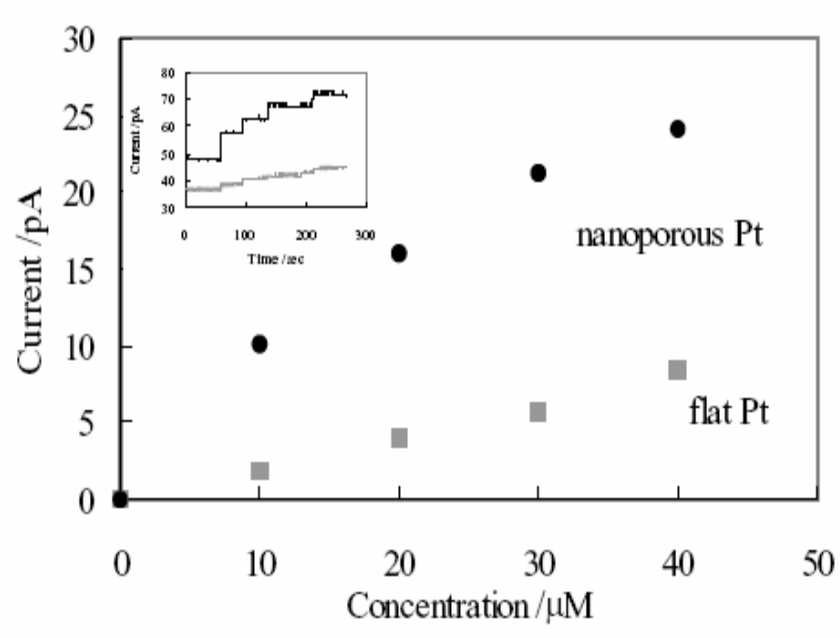

Figure 17. Calibration curves for amperometric detection of glutamate at enzymatic biosensor based on flat and nanoporous Pt. The diameter of the electrodes is 25 μm. The inset shows the raw signals from amperometric measurements.

4. Conclusions

Nanoporous Pt surface having numerous nanopores with diameter 3 nm exhibits the significant enhancement of redox current of aqueous H_2O_2. Owing to nanoporosity, the onset potential of H_2O_2 oxidation shifts in less positive direction. These phenomena can be rationalized by noting that the electrode surface area is expanded by several hundred folds and the novel geometric feature offers even more chances to interact with inner wall of the Pt surface. These properties can be used to make a microelectrode sensing aqueous H_2O_2. The electrocatalytic power of nanoporous Pt for H_2O_2 oxidation highlights at microelectrodes where the inbound flux is remarkably high compared with flat surface due to spherical diffusion. Immobilizing enzyme onto the nanoporous surface, one can extend its usefulness to a practical application to enzymatic microsensor. In this study, glutamate sensor was fabricated and tested to demonstrate how nanoporous Pt provide a good platform for microbiosensors.

Chapter Ⅳ. Nanoporous Platinum Thin Film as a Solid-State Reference Electrode for Miniaturized System

1. Introduction

Most of electrochemical experiments are conducted in either three-electrode cell or two-electrode cell. And electrochemical cells almost always require one or more reference electrode. Potentiostat circuit is designed to have bonding port with high input impedance, which is connected with reference electrode. Thus, negligible current is allowed to flow through the reference electrode. As a result, constant potential is maintained at the reference electrode side. That way the potential of the working electrode can be defined and controlled with respect to the reference electrode.

The internationally accepted primary reference[38] is the standard hydrogen electrode (SHE), or normal hydrogen electrode (NHE), which has all components at unit activity :

$$Pt/H_2(a=1)/H^+(a=1,\ aqueous\ )$$

Potentials are often measured and quoted with respect to reference electrodes other than the NHE, which is not very convenient for normal experiments. A common reference is the saturated calomel electrode (SCE), which is

$$Hg/Hg_2Cl_2/KCl\ (saturated\ in\ water)$$

Corresponding potential is 0.242 V vs. NHE. Another is the silver-silver

chloride electrode.

Ag/AgCl/KCl (saturated in water)

with a potential of 0.197 V vs. NHE.

Although many reference electrodes are developed and used commercially, most reference electrodes are macroscopic scale. Because miniaturization of the electrochemical sensor or micro-total-analysis-systems (μ-TAS) attracts scientists' attention now, smaller and simpler reliable reference electrode is very required. To date Ag/AgCl covered with a suitable protective layer[40-42] has been adopted by μ-TAS[39]. However, this system needs a protective layer because it is difficult to avoid dissolution of AgCl even in highly concentrated chloride solutions. Moreover, since the AgCl layer is insulating, the protective outer layer cannot be formed by electrochemical deposition, which is an appropriate method for miniaturized systems requiring the layers exclusively on the top of the tiny conducting spots of interest. Moreover, Ag/AgCl demands a constant chloride concentration, which is a less common condition than a constant pH.

Solid-state reference electrodes based on metal oxides have been addressed with the aim of developing potential alternatives to Ag/AgCl for miniaturized systems because metal oxides are favorable for conventional patterning processes and develop constant potential according to the pH of surround in principle. Unfortunately, most metal oxides are ostensibly suitable for solid-state pH sensors because they produce unstable and irreproducible potential in response to pH. As

pH-sensitive materials, they are suffering from non-Nerntian behavior, hysteresis, and interference from redox-active couples[21]. IrO_2 is the sole material that has been recommended by a number of reports owing to its low sensitivity to redox interference, low hysteresis, and potential stability over a wide pH range[43, 44].

This study suggests that nanoporous structure is possible as another alternative solid-state reference electrode. The nanoporous structure has advantage in aspect of polarizability over conventional flat electrodes.

The ideal reference electrode must have a non-polarizable interface, on which any particular current does not produce further over-potential. Bockris et al. mentioned that the equilibrium exchange current density, i_0 is a quantitative criterion of polarizability[45]. The electrode/solution interface becomes proportionally less polarizable as i_0 climbs. Therefore, i_0 should be sufficiently high to sustain a constant potential at the interface. Since the metal/metal oxide of a metal electrode involves a surface-confined reaction, it is predicted that i_0 should be linearly dependent on the surface area. The nanoporous surface structure enormously enlarges the area of metal oxide, which is exposed to solution in the nanopores. Accordingly, the exchange current, i_0, for nanoporous metal electrodes is expected to be much higher than that of flat electrodes.

According to previous paper[14] about pH response's performance of H_1-ePt, bare nanoporous platinum oxides exhibit near-Nernstian behavior (e.g., -55 mV/pH in PBS), ignorable hysteresis, a short response time,

and high precision, which are remarkably better than those of flat platinum oxides. The study strongly suggests the usefulness of nanoporous platinum in applications such as solid-state pH sensors.

The noble performance of nanoporous Pt as solid-state pH sensitive materials implies that the nanoporous Pt functions well as a reference electrode of electrochemical cell whose pH is kept constant. The following presents how nanoporous platinum oxide electrodes work as innovative solid-state reference electrodes, which are potentially useful for miniaturized electrochemical systems, such as for detection units on microfluidic chips.

Although L_2-ePt also shows perfect Nernstian responses and negligible hysteresis to pH change(Figure 18), H_1-ePt is applied in this reference electrode part due to convenience of electrodeposition on a chip. For example, electrodeposition of H_1-ePt can be carried out on a small spot without a storehouse, which is required to keep surfactant solution because of highly viscous liquid crystalline solution.

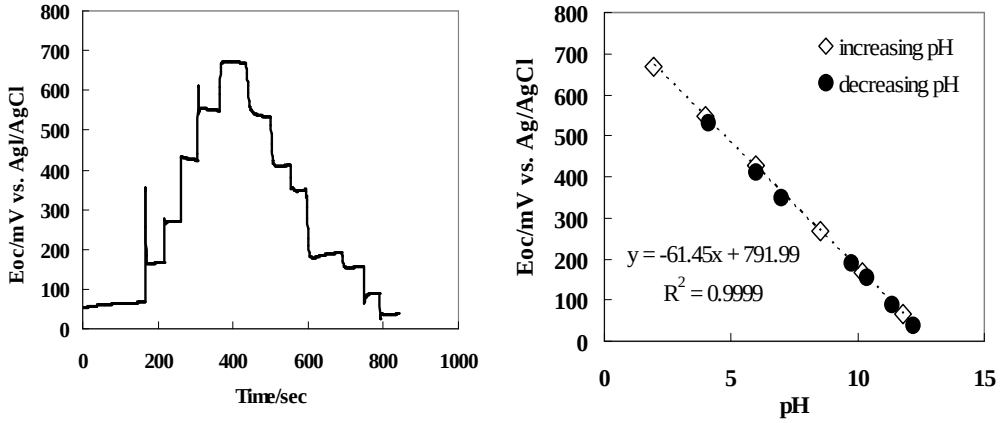

Figure 18. (A) Responses of L_2-ePt to pH changes in a stirred and air-saturated phosphate buffer solution. (B) E_{oc} versus pH curves. pH was decreased by adding 2 M H_3PO_4 to 0.1 M Na_3PO_4 (diamond) and then increased by adding 2 M NaOH again (circle).

2. Experimental

2.1 Reagents

Octaethylene glycol monohexadecyl ether, $C_{16}EO_{8,}$ (Fluka), hydrogen hexachloroplatinate hydrate (Aldrich), and 1,3-phenylenediamine (m-PD) dihydrochloride (Aldrich) were used without purification to fabricate nanoporous Pt and poly-m-PD layer. A negative, epoxy-type photoresist, SU8, and its developer from Microchem Corp. (Newton, MA, USA) were used to make the molds for PDMS channels. For patterning Pt electrode, hexamethyl disilane (HMDS) (J.T. Baker, Phillipsburg, NJ, USA), a positive photoresist, AZ5214-E), and its developer AZ300MIF (Clariant Corp., Muttenz, Switzerland) were used. Poly dimethyl siloxane (PDMS) slygard 184 was purchased from Dow-corning.

2.2 Instruments

Electrochemical experiments were performed using an electrochemical analyzer (Model CH660, CH Instruments Inc., Austin, TX 78733). Ag/AgCl (saturated KCl) and Hg/Hg_2SO_4 (saturated K_2SO_4) were used as a reference electrode and a platinum wire as a counter electrode. The substrate electrode for the nanoporous platinum film was a platinum disk electrode (0.020 cm^2). Another Pt disk electrode was polished with alumina (0.3 μm and 0.05 μm) and used as a flat Pt electrode.

2.3. Preparation of liquid crystals

$C_{16}EO_8$ (0.42 g), distilled water (0.29 g), and hydrogen hexachloroplatinate hydrate (0.29 g) were mixed, and the temperature was raised to 80 °C – the mixture then became transparent and homogeneous. Electrodes were then inserted into the homogeneous mixture and the mixture was cooled to room temperature (23 - 26 °C). At this stage, the mixture becomes a highly viscous liquid crystalline material.

2.4. Electrodeposition of nanoporous platinum and poly-m-PD

Platinum deposition was carried out on a polished platinum disk electrode at constant potential (-0.06 V vs Ag/AgCl) in liquid crystalline solution. The resulting nanoporous platinum electrode was placed in distilled water for 1 hr to extract the $C_{16}EO_8$, and the extraction procedure was repeated. The electrode was then electrochemically cleaned using a cycling potential between 0.68 and -0.72 V versus Hg/Hg_2SO_4 in 1 M sulfuric acid, until reproducible cyclic voltammograms were obtained. It is believed that hexagonally cylindrical porous structures of platinum (H_1-ePt) are formed during this procedure, as previously described[10, 46].

The electrochemical polymerization of 1,3-phenylenediamine (*m*-PD) was done using a previously described method[47, 48]. In brief, a thin

poly-*m*-PD layer was fabricated on a platinum oxide surface by five cyclic scans of potential between 0.6 and 1.0 V versus Ag/AgCl (saturated KCl) at 5 mV/s in a phosphate buffered saline (PBS) containing 10 mM *m*-PD

2.5. Fabrication of microfluidic chip

2.5.1. SU-8 mold for PDMS channel

In previous study[49], fabrication process of micro-chip is described. Corning 2947 slide glasses were used as substrates. After a slide glass was cleaned in pirana solution (H_2SO_4:H_2O_2=3:1) for 1 h, it was rinsed with DI water, acetone, methanol and DI water sequentially. The cleaned slide glass was baked on a hot plate at 150 ℃ to hydrate the surface for 10 min and was cooled to room temperature. HMDS(hexamethyl disilane) was coated by a spin-coater from Won Corporation as an adhesion promoter at 4000 rpm for 30 s and excessive solvent was vaporized by baking the glass on hot plate at 150 ℃ for 5 min.

SU8 on the cooled slide was spin-coated at 1800 rpm for 30 s which resulted in a 10 - 11 ㎛ thick SU8 film. Then, the SU8-coated slide glass was baked on hot plates in two steps: at 65 ℃ for 2 min and at 90 ℃ for 5 min. After cool-down, the slide was exposed to UV light (365 nm) with intensity of 16 mW/cm^2 for 10 s in a mask aligner, MDE-4000, from Midas system Co. Ltd. (Daejeon, Korea) using a channel patterned

mask and was baked again at 65 ℃ for 1 min and at 90 ℃ for 2 min. Then, the cooled slide was developed with SU8 developer for~1 min under close monitoring. After careful rinse with isopropyl alcohol and DI water, the SU8 pattern on the slide was cured on a hot plate at 175 ℃ for 2 h to facilitate surface adhesion.

For preparation of the PDMS layer with pattern of the channels, one part of the curing agent was added to 10 parts of the PDMS base. After mixing them carefully, the mixture was degassed in a vacuum chamber for 30 min. Then, the PDMS mixture was poured onto the prepared SU8 mold. The PDMS was thermally cured at 62 ℃ for 2 h.

2.5.2. Metal electrodes and assembly

A Corning 2947 slide glass was cleansed and HMDS-coated as previously described. Then, AZ5214-E was spin-coated at 2000 rpm for 30 min and was baked at 100 ℃ for 1 min. The PR coated slide exposed to UV light (365 nm) with intensity of 16 mW/cm^2 for 5 s using an electrode-patterned mask and was baked at 100 ℃ for 5 min. For image reversal, PR on the slide was flooded with UV radiation for 15 s. The pattern was developed with AZ300MIF for ~1 min under close monitoring and rinsed with DI water.

The glass slide was dried by air-blowing. Twenty nanometers thick Ti and 100 nm thick Pt layers were sequentially deposited by a Radio Frequency Magnetron sputter system from Atek systems (Incheon,

Korea). Then, the Ti/Pt layer was soaked into acetone and lift-off with the aid of sonication in 3510E-DTH from Bransonic (Danbury, CT, USA) for 5 min. The areas of working, reference, and counter electrodes were 0.00785 cm^2, 0.00343 cm^2, and 0.0314 cm^2 respectively. The PDMS layer with a microchannel pattern was attached on the Pt-mounted slide glass.

2.6. Electrodeposition of Ag and AgCl on a working electrode spot in a chip

PDMS chamber was attached to working electrode spot around so as to expose only electrode surface to solution. Working Pt electrode was electrochemically cleaned in poured 1 M H_2SO_4 in a PDMS chamber until typical cyclic voltammogram of platinum is appeared. And electroplating of Ag was conducted by bulk electrolysis at 0.0 V versus Hg/Hg_2SO_4 in 100 mM KNO_3 containing 10 mM $AgNO_3$ up to 2.8 C/cm^2. To electrodeposit AgCl on a Ag deposited working electrode spot, anodic current (0.4 mA/cm^2) was passed by using chronopotentiometric technique in saturated KCl solution for about 4000 s. The color of AgCl plated on Ag has dark gray.

3. Results and Discussions

3.1. Effect of nanoporous structure

Figure 19 shows the results of chronopotentiometry conducted with H_1-ePtO and flat PtO. Constant anodic (1 μA/cm^2) current was allowed to flow until 1000 s. The potential change of H_1-ePtO (79 mV) is much slower than that of flat PtO (378 mV) for 1000 s. It tells that E_{oc} of H_1-ePt upon a galvanostatical current undergoes even smaller change than that of flat Pt. This indicates the high nonpolarizability of H_1-ePtO, which is originated from its extremely high surface area.

This advantage of high nonpolarizability is more clear in two-electrode system, especially consisting of microelectrode. In this system, E_{oc} of a micro flat Pt electrode as a reference electrode is expected to be unstable because high current density will be imposed on the small electrode area. On the other hand, the E_{oc} of a micro H_1-ePt electrode is more stable and steady owing to its high nonpolarizability.

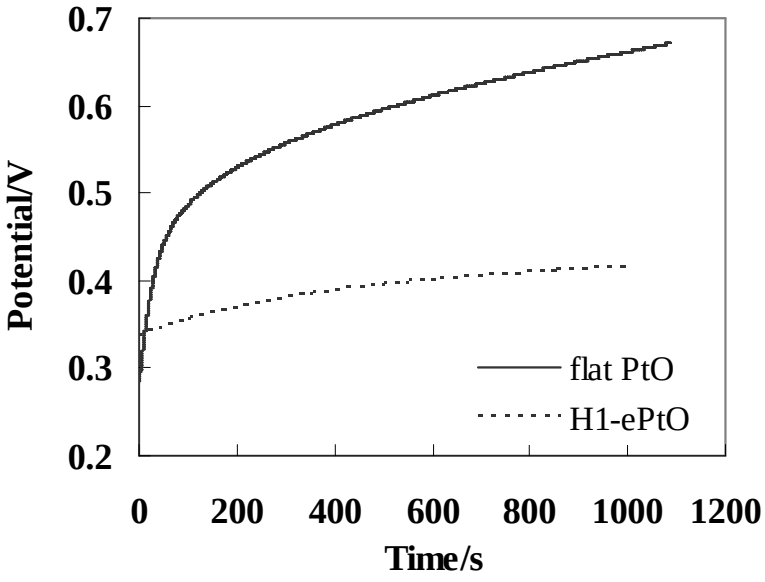

Figure 19. Results of choronopotentiometry for H_1-ePtO (dotted) and flat PtO (solid), under constant current condition of 1 μA/cm^2, in PBS solution (pH 7.4).

3.2. Effect of a redox couple in the solution

Figure 20 shows the open-circuit potentials(E_{oc}) of H_1-ePtO (figure 20B) and flat PtO (figure 20A) in PBS buffer with or without redox couple. Figure 20A shows that the E_{oc} of flat PtO is very sensitive to the presence of the $Fe(CN)_6^{3-/4-}$ redox couple. This is commonly found for most metal oxides. Fog et al. reported that platinum oxide was most sensitive to the $Fe(CN)_6^{3-/4-}$ couple among the metal oxides they tested[21]. The surface potential of flat Pt is mainly determined by the redox equilibrium of the $Fe(CN)_6^{3-/4-}$ couple.

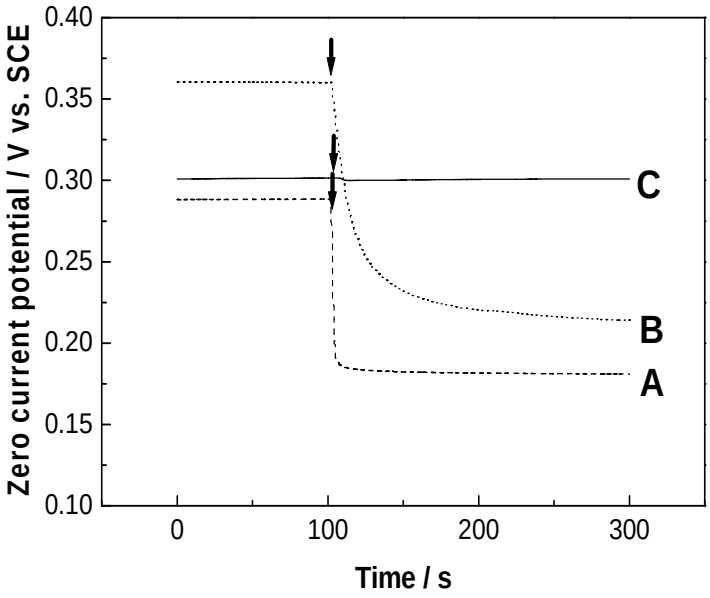

Figure 20. Chronopotentiometric curves of (A) flat PtO, (B) H_1-ePtO (r.f. 318), and (C) H_1-ePtO/poly-*m*-PD (r.f. 236) to added $Fe(CN)_6^{3-/4-}$ in aerated and stirred PBS solution (pH 7.3). The concentrations of $K_3Fe(CN)_6$ and $K_4Fe(CN)_6$ were increased from 0 to 0.5 mM at 100 s (indicated by arrows) by injecting their concentrated solutions.

On the other hand, the response of H_1-ePtO is quite different to that of flat PtO, as shown in Figure 20B. Although the E_{oc} is still seriously affected by the $Fe(CN)_6^{3-/4-}$couple, the contribution of Pt/PtO grows markedly. This result indicates that the surface equilibrium of Pt/PtO is not a minor factor in determining the E_{oc}'s of electrodes with nanoporous structures. This is not surprising when it is borne in mind that the exchange current of nanoporous Pt/PtO increases enormously as the surface area is increased. Meanwhile the exchange current due to $Fe(CN)_6^{3-/4-}$ climbs slowly compared with that of Pt/PtO because the contribution of the electrochemical reaction of $Fe(CN)_6^{3-/4-}$ does not increase as much as the surface contribution[13]. Therefore the results in Figure 20 indicate that the nanoporous surface morphology suppresses the relative contribution of $Fe(CN)_6^{3-/4-}$ to the E_{oc}, though it remains far from perfect.

3.3. Stabilities of platinum oxide electrodes

In order to check the stability of nanoporous Pt/PtO, the sensitivity of the E_{oc} to pH was monitored for several days. The E_{oc} of H_1-ePtO was maintained for at least 6 days. The average potential (pH 7.3) was 0.367 V versus SCE with a standard deviation of 0.011 V (n=4). The E_{oc} of flat PtO was so unstable that the standard deviation reached 0.028 V for an average value of 0.319 V over the same period. H_1-ePtO coated with poly-*m*-PD also showed stable potential average of 0.327 V and a

standard deviation of 0.006 V.

3.4. Effect of poly-m-PD layer

As Figure 20 shows, H_1-ePtO is less sensitive to the $Fe(CN)_6^{3-/4-}$couple than flat PtO. However the presence of $Fe(CN)_6^{3-/4-}$ still affects its sensitivity to pH. In order to eliminate the interference by redox couples more effectively, a compact nonconducting polymer (poly-*m*-PD) was applied. Figure 20C shows that the poly-*m*-PD layer is an excellent barrier to stop redox couples while the flat PtO instantly responds to the addition of a $Fe(CN)_6^{3-/4-}$ couple. Although H_1-ePtO shows a slower response to the redox couple than flat PtO, the redox couple retains a strong influence. However, the H_1-ePtO/poly-*m*-PD exhibits almost no response to the redox couple. This result indicates that H_1-ePtO/poly-*m*-PD is a promising candidate for practical reference electrodes in neutrally buffered aqueous solutions, such as biofluids.

3.5. Performance in voltammetry

In order to prove the performance of H_1-ePtO/poly-*m*-PD as a reference electrode, the results of voltammetric measurements using H_1-ePtO/poly-*m*-PD were compared with those using a SCE. Cyclic voltammograms obtained with SCE and H_1-ePtO/poly-*m*-PD had identical shapes with an $E_{1/2}$ difference of 0.30 V, as demonstrated in

Figure 21.

3.6. Performance in potentiometry

The performance of H_1-ePtO/poly-*m*-PD as a reference electrode was also demonstrated in potentiometric application using Ag/AgCl wire as indicator electrode for chloride ion (solid circle in figure 22). The Ag/AgCl indicator electrode acts as a typical chloride ion-selective electrode in combination with H_1-ePtO/poly-*m*-PD. The supplementary study showed that H_1-ePtO/poly-*m*-PD rarely showed the interference from chloride below the concentration of 0.1 M. Thus, the potentiometric system composed of Ag/AgCl and H_1-ePtO/poly-*m*-PD performs as a good chloride ISE over corresponding concentration range.

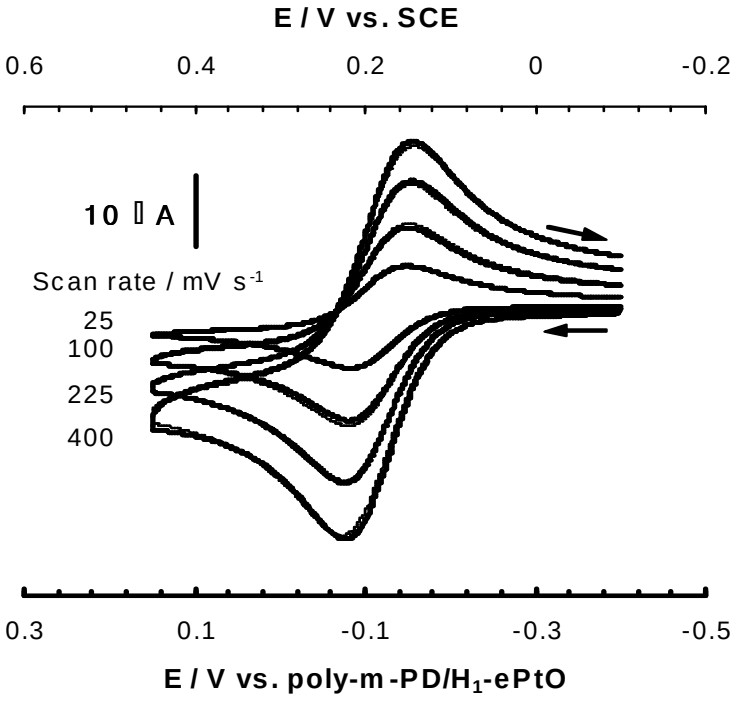

Figure 21. Cyclic voltammograms obtained in PBS containing 0.5 mM $K_3Fe(CN)_6$ and 0.5 mM $K_4Fe(CN)_6$, using a glassy carbon disk electrode (area: 0.071 cm^2) as a working electrode and SCE (thin line) or H_1-ePtO/poly-*m*-PD (r.f. 236) (thick line) as a reference electrode.

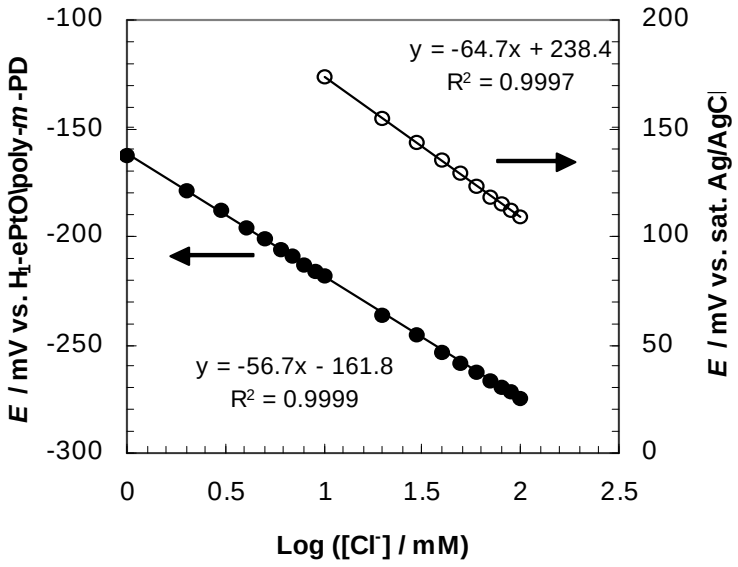

Figure 22. Potentiometric response obtained in phosphate buffer (0.15 M, pH 7.4) as increasing chloride concentration up to 0.1 M. AgCl on Ag wire (Ag/AgCl) was used as an indicator electrode. And H_1-ePtO/poly-*m*-PD (r.f. 100) or Ag/AgCl (saturated KCl) was used as a reference electrode.

3.7. Application for microchip

Microchip equipped with micro-electrochemical cell based on H_1-ePtO/poly-*m*-PD was constructed (figure 23). The micro-electrochemical cell contains three platinum electrodes, on which various surface modifications may be performed. For the application in voltammetry, H_1-ePtO/poly-*m*-PD was formed on the electrode 2, and all the three electrode were used (type A). For potentiometry, electrode 2 and 3 are coated with H_1-ePtO/poly-*m*-PD and Ag/AgCl respectively, and then only the two electrodes were used as two-electrode system (type B).

The performance of the micro-electrochemical cell equipped with H_1-ePt/poly-*m*-PD as solid-state reference electrode was tested in voltammetry and potentiometry. Figure 24A shows the cyclic voltammograms measured in A-type micro-electrochemical cell. The cyclic voltammograms show typical behaviors reported by the previous study for the similar micro-electrochemical cell with Ag/AgCl, which was isolated with polyelectrolyte salt bridge, as reference electrode[50].

Figure 24B shows the potentiometric response measured with type-B electrochemical cell. It shows that the H_1-ePtO/poly-*m*-PD embedded in micro-chamber together with Ag/AgCl performs as a good reference electrode like it acts in bulk electrochemical cell (figure 22). The voltammetric and potentiometric application of H_1-ePtO/poly-*m*-PD illustrates the usefulness for microanalysis system of solid-state

reference electrode, especially nanoporous platinum.

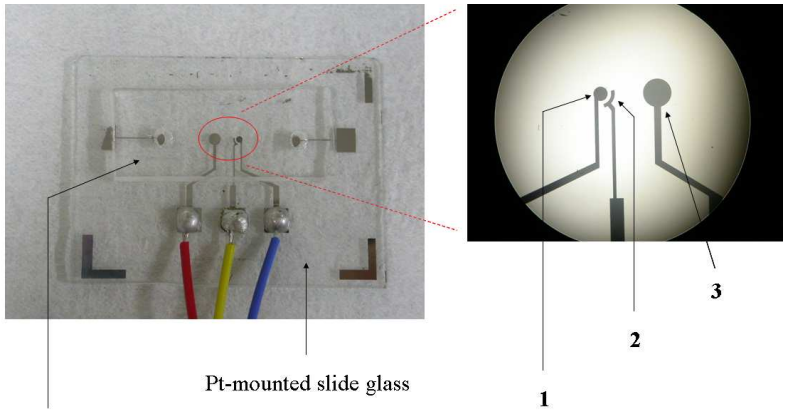

	1	2	3
Type-A	Flat Pt	H_1-ePtO\poly-*m*-PD	Flat Pt
Type-B	Dummy	H_1-ePtO\poly-*m*-PD	Ag/AgCl

Figure 23. The microchip (up) and the micro-electrochemical cell (bottom). The micro-elctrochemical cell was consisted with three Pt electrode; electrode 1 (0.00785 cm^2), 2 (dia. 0.00343 cm^2), and 3 (0.0314 cm^2). The electrochemical cell has two chambers, and electrode 1 and 2 are in the same chamber. The height of the chambers was 30 μm, and the chambers are connected by micro-channel whose height and width are 30 μm.

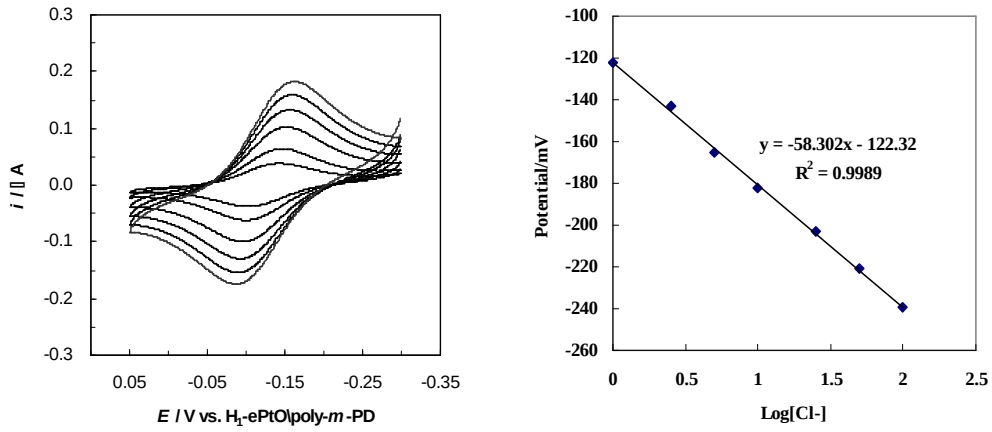

(A) (B)

Figure 24. Performance of H_1-ePtO/poly-*m*-PD as reference electrode embedded in microchannel during voltammetric (A) and potentiometric (B) mesearements. (A) Cyclic voltammogram of 0.5 mM ferricyanide and 0.5 mM ferrocyanide in PBS (pH 7.4) using Pt's (electrode 1 and 3) deposited by sputtering as working and counter electrodes. Scan rate; 1, 2, 4, 6, 8, 10 mV/s. (B) E_{oc} obtained in phosphate buffer (0.15 M, pH 7.4) as increasing chloride concentration up to 0.1 M. Ag/AgCl electroplated on electrode 3 and H_1-ePtO/poly-*m*-PD on 2 were used as an indicator and a reference electrode, respectively

4. Conclusions

This study shows a good possibility of nanoporous platinum structure for solid-state reference electrode. Nanoporous structure has enormously large surface area due to a great many of nanopores with 2-3 nm diameter. Exchange current for the surface equilibrium reaction of Pt/PtO is proportionate to electrode surface area. So, exchange current of the nanoporous Pt is much greater than the flat Pt. Accordingly, nanoporous Pt maintains the more stable open circuit potential in constant pH condition.

Interference from redox couples can be completely eliminated by appropriate blocking layers. The deposited poly-*m*-PD layer presents an example of the successful suppression of the effect of the $Fe(CN)_6^{3-/4-}$ couple.

H_1-ePtO/poly-*m*-PD system provides several valuable opportunities for various electrochemical applications, for example, chemical/biosensors and micro total analysis systems. It is easy to make and it takes only a short time to fabricate reproducible products, thus favoring mass production. Moreover, H_1-ePtO/poly-*m*-PD can be patterned in a small scale because its fabrication procedure is based on electrochemical methods. It is believed that H_1-ePt/*m*-PD system as solid-state reference electrode is potentially useful for miniaturized electrochemical systems, such as the electrochemical detection units integrated in microfluidic chips.

Reference

1. G. Binnig, H. Rohrer, *Angew. Chem. Int. Ed. Engl.* **1987**, 26, 606

2. J.-S. Ye, Y. Wen, W. De Zhang, L. Ming Gan, G. Q. Xu, F.-S. Sheu, *Electrochemistry Communication*, **2004**, *6*, 66.

3. S. E. Moulton, A. I. Minett, G. G. Wallace, *Sensor Letters*, **2005**, *3*, 183.

4. C. H. Yen, X. Cui, H.-B. Pan, S. Wang, Y. Lin, C. M. Wai, *J. Nanosci. Nanotechnol*, **2005**, *5*, 1852.

5. D. Sun. S. A. Rocks, M. J. Edirisinghe, R. A. Dorey, Y. Wang, *J. Nanosci. Nanotechnol*, **2005**, *5*, 1846.

6. Barreca, Davide. Gasparotto, Alberto, Maragno, Cinzia, Tondello, Eugenio, *J. Nanosci. Nanotechnol*, **2005**, *5*, 1883.

7. Endo, Takeshi, Kuno, Takehito, Yoshimura, Tomokazu, Esumi, Kunio, *J. Nanosci. Nanotechnol*, **2005**, *5*, 1875.

8. W. G. Pell, B. E. Conway, *J. Power Sources*, **1996**, *63*, 255.

9. J. Wang, L. Agens, *Anal. Chem.* **1992**, *4*, 456.

10. G. S. Attard, P. N. Bartlett, N. R. B. Coleman, J. M. Elliott, J. R. Owen, J. H. Wang, *Science* **1997**, *278*, 838.

11. K.-S. Choi, E. W. McFarland, G. D. Stucky, *Advanced Materials* **2003**, *15*, 2018.

12. L. Coppola, C. La Mesa, G. A. Ranieri, M. Terenzi, *J. Colloid Interface Sci.* **1991**, *147*, 517.

13. S. Park, T. D. Chung, H. C. Kim, *Anal. Chem.* **2003**, *75*, 3046.

14. S. Park, H. Boo, Y. Kim, J.-H. Han, H. C. Kim, T. D. Chung, *Anal. Chem.* **2005**. *77*, 7695

15. P. R. Birkin, J. M. Elliott, Y. E. Watson, *Chem. Commun*, **2000**, 1693

16. S. A. G. Evans, J. M. Elliott, L. M. Andrews, P. N. Barttlet, P. J. Doyle, G. Denualt, *Anal. Chem.* **2002**, *74*, 1322

17. A. Kucernak, J. Jiang, *Chemical Engineering Journal*, **2003**, *93*, 81

18. S. Park, H. Boo, T. D. Chung, *Anal. Chim. Acta* in press.

19. A. J. Bard, L. R. Faulkner, Electrochemical methods: Fundamentals and Applications Wiley: New York, **2001**.

20. J. O. M. Bockris, A. K. N. Reddy, Modern Electrochemistry Plenum: New York, **1973**.

21. Fog, A.; Buck, R. P. *Sens. Actuators*. **1984**, *5*, 137

22. S. Trasatti, O. A. Petrii, *J. Electroanal. Chem.* **1992**, *327*, 353

23. P. N. Bartlett, J. J. Baumberg, P. R. Birkin, M. A. Ghanem, M. C. Netti, *Chem. Mater.* **2002**, *14*, 2199

24. B. Gollas, J. M. Elliott, P. N. Bartlett, *Electrochim. Acta*. **2000**, *45*, 3711.

25. I. Nandhakumar, J. M. Elliott, G. S. Attard, *Chem. Mater*. **2001**, *13*, 3840.

26. P. A. Nelson, J. M. Elliott, G. S. Attard, J. R. Owen, *Chem. Mater*. **2002**, *14*, 524.

27. K.-L. Yang, S. Yiacoumi, C. Tsouris, *Nano Lett*. **2002**, *2*, 1433.

28. H. Boo, S. Park, B. Ku, Y. Kim, J. H. Park, H. C. Kim, T. D. Chung, *J. Am. Chem. Soc,* **2004**, *126*, 4524.

29. P. Westbroek, B. Van Huate, E. Temmerman, J. Fresenius, *Anal. Chem.* **1996**, *354*, 405.

30. K. Aoki, M. Ishida, K. Tokuda, K. Hasebe, *J. Electroanal. Chem. Interfacial Electrochem.* **1988**, *251*, 63.

31. S. B. Hall, E. A. Khudaish, A. L. Hart, *Electrochim. Acta* **1998**, *43*, 579.

32. S. B. Hall, E. A. Khudaish, A. L. Hart, *Electrochim. Acta* **1998**, *43*, 2015.

33. S. B. Hall, E. A. Khudaish, A. L. Hart, *Electrochim. Acta* **1999**, *44*, 2455.

34. S. B. Hall, E. A. Khudaish, A. L. Hart, *Electrochim. Acta* **1999**, *44*, 4573.

35. S. B. Hall, E. A. Khudaish, A. L. Hart, *Electrochim. Acta* **2000**, *45*, 3573.

36. B. A. Morrow, W. A. Clark, R. H. Roth, *Eur. J. Pharmacol.* **1993**, 238, 255.

37. M. E. Wolf, *Prog. Neurobiol.* **1998**, *54*, 697.

38. Bard, A. J.; Faulkner, L. R. Electrochemical methods: Chapter 1. Introduction and overview of electrode processes.

39. E. Dempsey, D. Diamond, M. R. Smyth, G. Urban, G. Jobst, I. Moser, E. M. J. Verpoorte, A. Manz, H. M. Widmer, K. Rabenstein, R. Freaney, *Anal. Chim. Acta* **1997**, *346*, 341.

40. H. Suzuki, *Electroanalysis* **2000**, *12*, 703.

41. A. M. Nolan, S. H. Tan, S. P. Kounaves, *Anal. Chem.* **1997**, *69*,

1244.

42. H. J. Lee, U. S. Hong, D. K. Lee, J. H. Shin, H. Nam, G. S. Cha, *Anal. Chem.* **1998**, *70*, 3377.

43. A. N. Bezbaruah, T. C. Zhang, *Anal. Chem.* **2002**, *74*, 5726.

44. S. A. M. Marzouk, *Anal. Chem.* **2003**, *75*, 1258.

45. J. O. M. Bockris, A. K. N. Reddy, Modern electrochemistry Plenum: New York, **1973**; Vol. 2.

46. J. M. Elliott, G. S. Attard, P. N. Bartlett, N. R. B. Coleman, D. A. S. Merckel, J. R. Owen, *Chem. Mater.* **1999**, *11*, 3602.

47. R.-A. Jeong, J. Y. Hwang, S. Joo, T. D. Chung, S. Park, S. K. Kang, W.-Y. Lee, H. C. Kim, *Biosens. Bioelecron.* **2003**, *19*, 313.

48. T. D. Chung, R.-A. Jeong, S. K. Kang, H. C. Kim, *Biosens. Bioelecron.* **2001**, *16*, 1079.

49. S. K. Kim, H. Lim, T. D. Chung, H. C. Kim, *Sensors and Actuators B*. in press.

Abstract

The Electrocatalytic effect of Nanoporous Surface and its Applications

Ji-Hyung Han
Department of chemistry
Graduate school of
Sungshin Women's University

Nanoporous metal surfaces in this study are composed of numerous nanopores with diameter of 3 nm. Because of this unique structure, it is expected that active real surface and collision frequency could be remarkably enhanced. We investigated the apparent electrocatalysis that is observed at the nanoporous electrodes in terms of collision frequency as well as surface area. Based on the fundamental research on the origin of the apparent electrocatalytic behavior, two practical applications including micro-glutamate sensor and solid-state reference electrode were demonstrated. Overall, this thesis consists of three parts with respective issues as follows.

Part I addressed the novel structural effect of nanoporous platinum surface to the amperometric responses to glucose and hydrogen peroxide, and potentiometric signals due to pH changes. Geometric effect of

nanopores was verified in both faradaic reaction of sluggish glucose oxidation and non-faradaic system of open circuit potential responding to any pH change.

In part Ⅱ, the apparent catalytic ability of nanoporous platinum was exploited to develope enzymatic glutamate micro-sensor. The oxidation current of hydrogen peroxide generated in enzymatic reaction was amplified by nanoporous platinum, which had been electroplated on a Pt/Ir alloy wire. 1,3-phenylenediamine was electropolymerized on the electrode for immobilization of glutamate oxidase (GLOx). The sensitivity of nanoporous platinum for glutamate was four times higher than that of flat platinum.

Part Ⅲ reported the utilization of nanoporous platinum for a new kind of solid-state reference electrode. The anodized nanoporous platinum provides many electroanalytical characteristics such as near-nerntian behavior, low hysteresis, and a short response time in pH response that suggest the application to a solid-state reference electrode in a constant pH condition. In addition, Poly-*m*-PD layer on nanoporous platinum oxide effectively suppresses the interferences by redox-active species, which are often serious problems in the conventional IrO_x system. It was showed that the solid-state reference electrode of poly-*m*-PD coated nanoporous platinum can be successfully integrated in the microfluidic system on a glass chip.

감사의 글

아무 것도 모르고 연구실에 들어 온지가 엊그제 같은데, 벌써 졸업을 하게 되었습니다. 부족한 저를 격려해 주시고 가르쳐 주신 정택동 교수님께 먼저 감사의 말씀을 드립니다. 교수님이 말씀하신 것처럼, 큰 꿈으로 꾸고, 자신감을 가지고 살겠습니다. 그리고 힘든 일로 주저하거나 포기하지 않고 앞으로 나아가겠습니다. 항상 지켜봐 주세요.

학부 생활 동안 가르침을 주신 유은아 교수님, 정선호 교수님, 정미원 교수님, 박성순 교수님께 감사드립니다. 그리고 직접 친절하게 실험 지도를 해주시고, 전기화학적 지식을 가르쳐 주신 박세진 박사님, 부한길 박사님께 감사드립니다. 덤벙대는 저에게 생각하는 습관을 가르쳐 주셔서 정말 감사해요. 박사님들 덕분에 전기화학에 대해서 정말 많은 것을 배우게 되었습니다.

칩 만드느라 고생하신 종민 오빠, 저를 외계인이라고 항상 놀리시는 상학 오빠, 세경 오빠께 감사드립니다. 학부 때 제일 무서웠던, 하지만 연구실에선 다정다감하시고 예쁘신 본경 언니, 정말 감사드리고, 언니 닮은 예쁜 아기 낳으세요. 그리고 말 안 듣는 저 때문에 많이 고생하셨던 효진 언니, 가끔씩 정말 무섭지만 너무나 귀여우신 윤미 언니, 카리스마 선영 언니, 모두 감사 드려요. 선배님들이 있었기에 대학원 생활동안 많은 것을 배우게 됐어요. 더 좋은 후배가 되도록 노력하겠습니다. 끊임없는 질문에 가끔씩 난감해 하시지만 제가 이해하기 쉽게 말씀해 주시고, 때로는 고민을 상담해 주시는 정말로 착하신 란아 언니, 정말 감사 드려요. 언니 없었으면 졸업 못했을 거예요. 그리고 내 후배들… 조교로서 선망의 대상인 연주, 웃는 모습이 귀여운 범진아. 정말 고마워. 우리 연구실을 부탁한다. 자주 뭉치지 못해서 아쉬웠던 동기들.. 선자, 윤정이, 지선이, 유나, 혜용아, 좋은 논문 쓰길 바랄께. 그리고 알고 보면 터프한 연경 언니에게도 감사의 말씀 드립니다. 연식군, 나 때문에 고생 많이 했다. 좋은 여자 친구 생기길.. 그리고 열심히 대학원 생활하는 지영아. 좋은 논문 쓰고 얼굴 좀 자주 보자.

대학원 생활로 힘들어 하던 나를 격려해주고 챙겨줬던 승근아, 정말 고마워. 앞으로

네가 하는 일 다 잘 될꺼야. 그리고 나의 귀염둥이 동생들… 효정아, 승민아, 항상 웃으면서 커야 한다.

마지막으로 저를 지금껏 키워 주시고, 항상 걱정해주시는 부모님께 감사하다는 말씀을 드립니다. 항상 건강하세요. 행복하세요. 제가 부모님 곁을 든든하게 지켜드리겠습니다.

2006년 6월 논문을 마무리하며

한 지 형 올림